Search for stochastic gravitational-wave background

Kin-Wang Ng (吳建宏)

Institute of Physics &
Institute of Astronomy and Astrophysics
Academia Sinica, Taiwan

The Future is Illuminating

NTHU, Hsinchu, Taiwan

June 28 – 30, 2022

+ Guo-Chin Liu (Tamkang University)
+ Yu-Kuang Chu (AS → UW Milwaukee)
+ Reggie Bernardo (AS)

Outline

- Stochastic gravitational-wave background (GWB)
- Astrophysical and cosmological sources
- Observation
- Data pipelines (for an example, see Bernardo's talk)
- Our works to lay out a scheme for a fast computation of the detector responses (ORFs) to polarized GWB
- Conclusion

Cosmological GW spectral energy density

tion h_{ij} is gauged to be transverse-traceless. The latter can be decomposed into two polarization unit tensors as

$$h_{ij}(\eta, \vec{x}) = \sum_{\lambda=+,\times} \int \frac{d^3\vec{k}}{(2\pi)^{\frac{3}{2}}} h_\lambda(\eta, \vec{k}) \epsilon_{ij}^{\lambda}(\hat{k}) e^{i\vec{k}\cdot\vec{x}}, \qquad (2)$$

where $h_\lambda(\eta, \vec{k})$ is a Gaussian random field that defines the power spectrum of tensor perturbation,

$$\langle h_\lambda(\eta, \vec{k}) h^*_{\lambda'}(\eta, \vec{k}') \rangle = \delta(\vec{k} - \vec{k}') \frac{2\pi^2}{k^3} \mathcal{P}_h^{\lambda\lambda'}(\eta, k). \qquad (3)$$

In the following, we will assume that $\mathcal{P}_h^{\lambda\lambda'}(\eta, k) = \delta_{\lambda\lambda'} \mathcal{P}_h(\eta, k)$. Then, the spectral energy density of the GWs relative to the critical density is given by

$$\Omega_{\rm GW}(\eta, k, \hat{k}) \equiv \frac{k}{\rho_c} \frac{d\rho_{\rm GW}}{dk d^2\hat{k}} = \frac{1}{96\pi} \left(\frac{k}{aH} \right)^2 \bar{\mathcal{P}}_h(\eta, k), \quad (4)$$

where $\rho_c = 3M_p^2 H^2$ and the overbar denotes taking a time-average. For k-modes that re-enter the horizon

Cosmological sources for gravitational waves

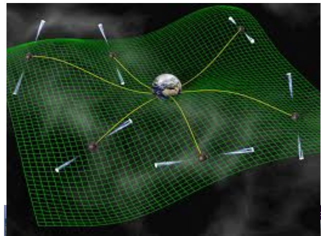

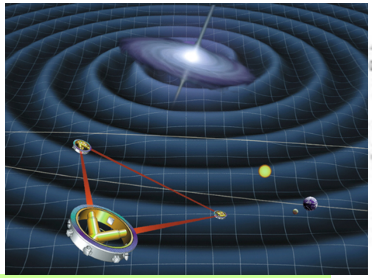

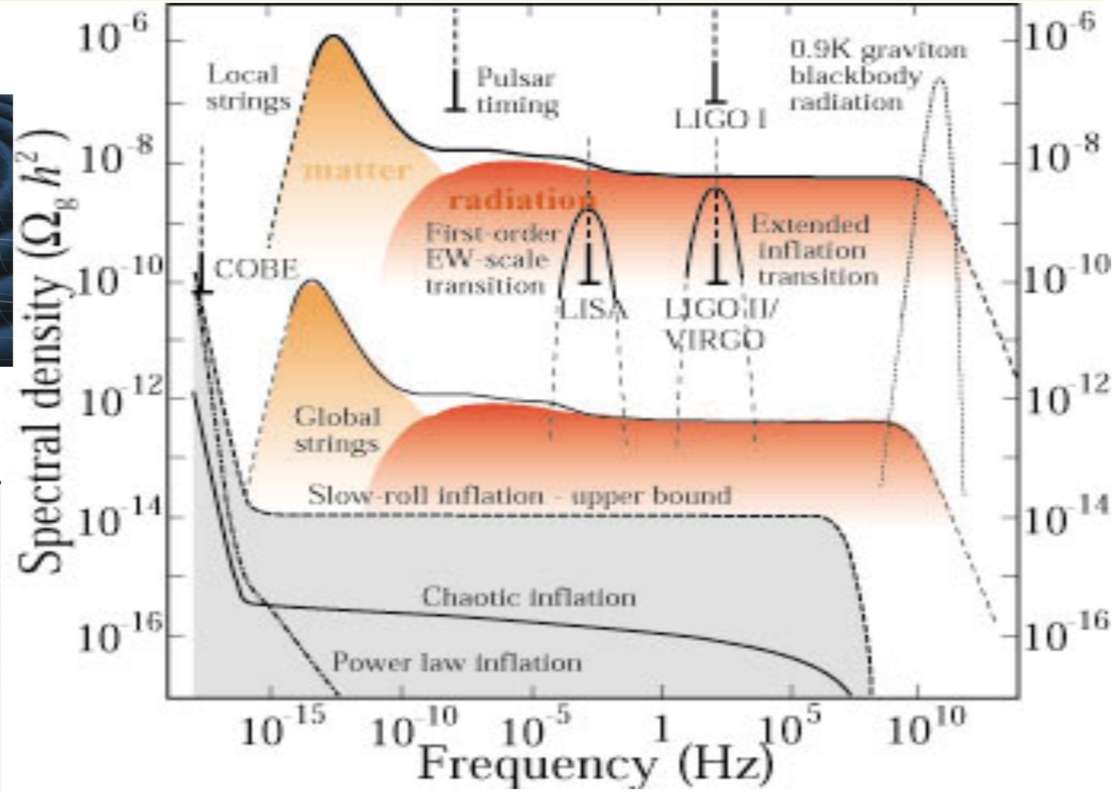

Astrophysical sources

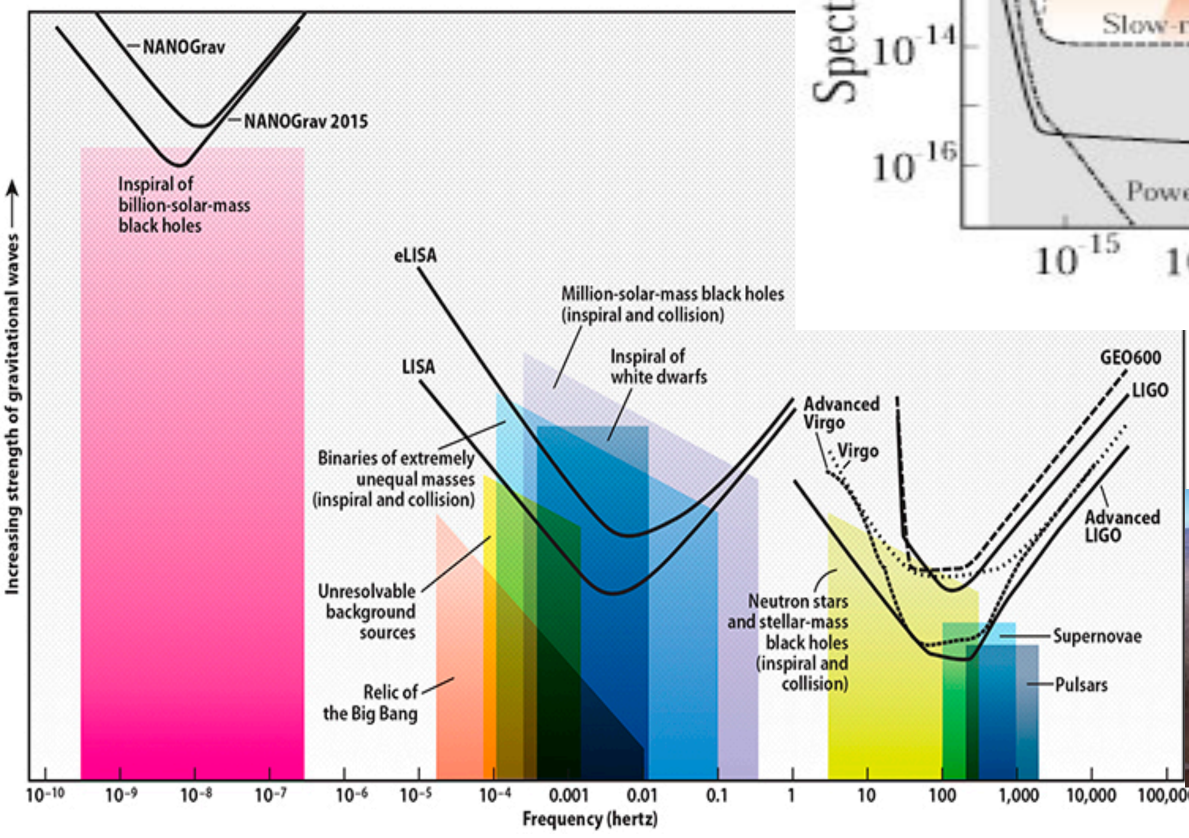

Current Upper Bounds

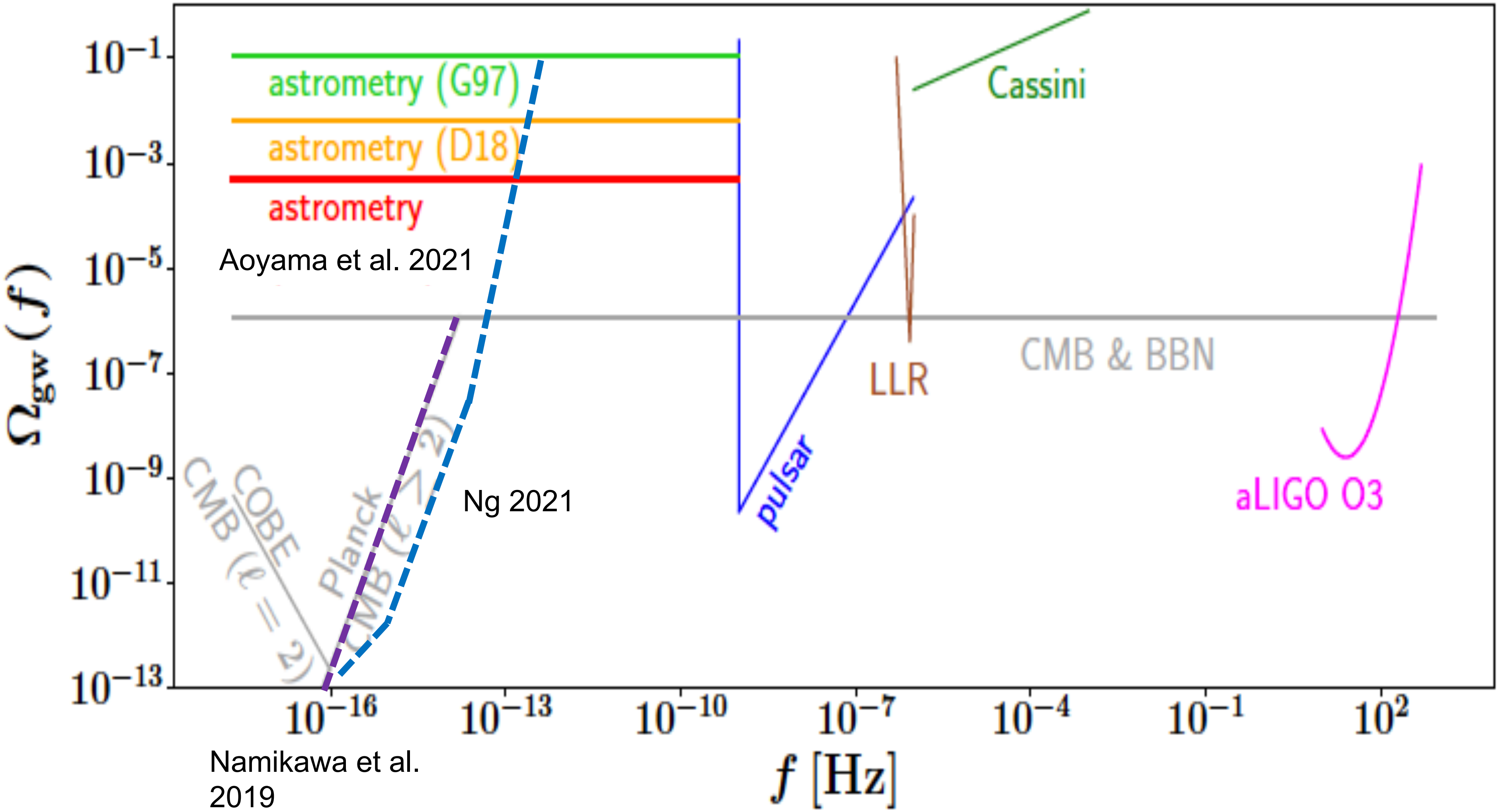

CMB&BBN – extra degrees of freedom
Cassini+LLR – radar launching

CMB – anisotropy + B-mode polarization
aLIGO – direct detection of wave strain
Pulsar – Shapiro time delay
Astrometry – gravitational lensing effect

Planck CMB Anisotropy $D^{TT}_l = l(l+1)\, C^T_l$ 2018

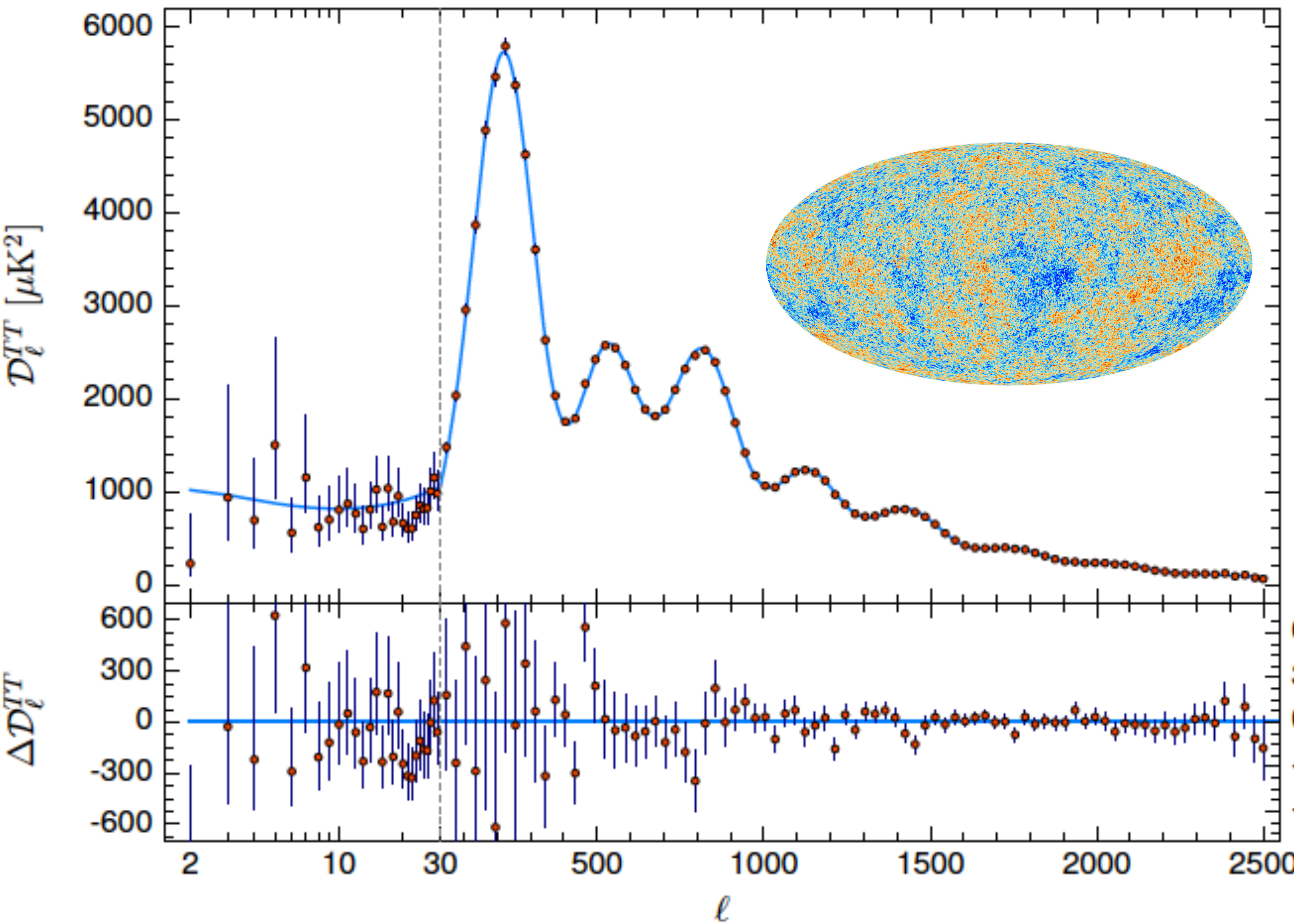

Planck CMB Polarization Power Spectra 2018

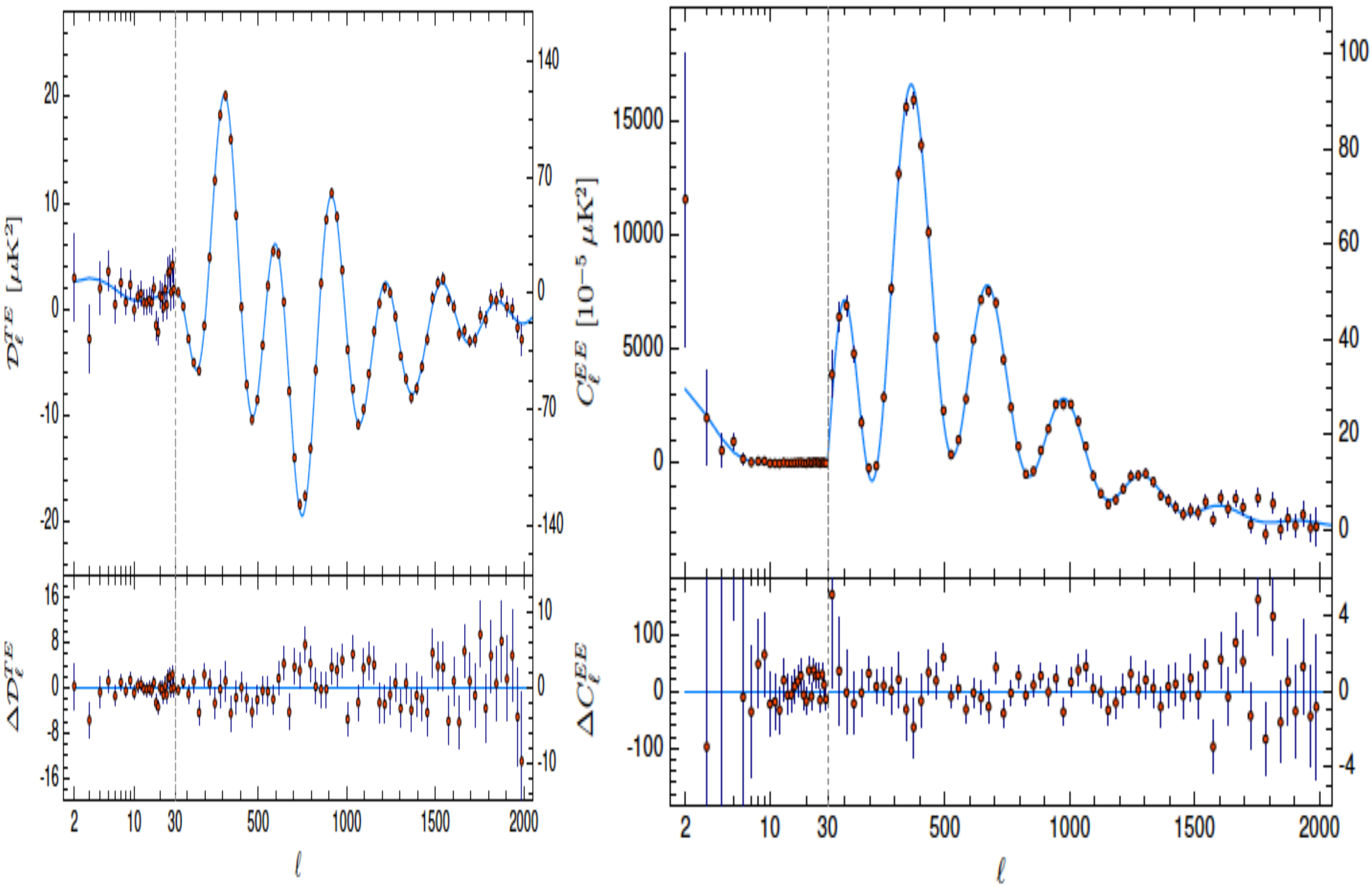

Latest small-scale CMB measurements

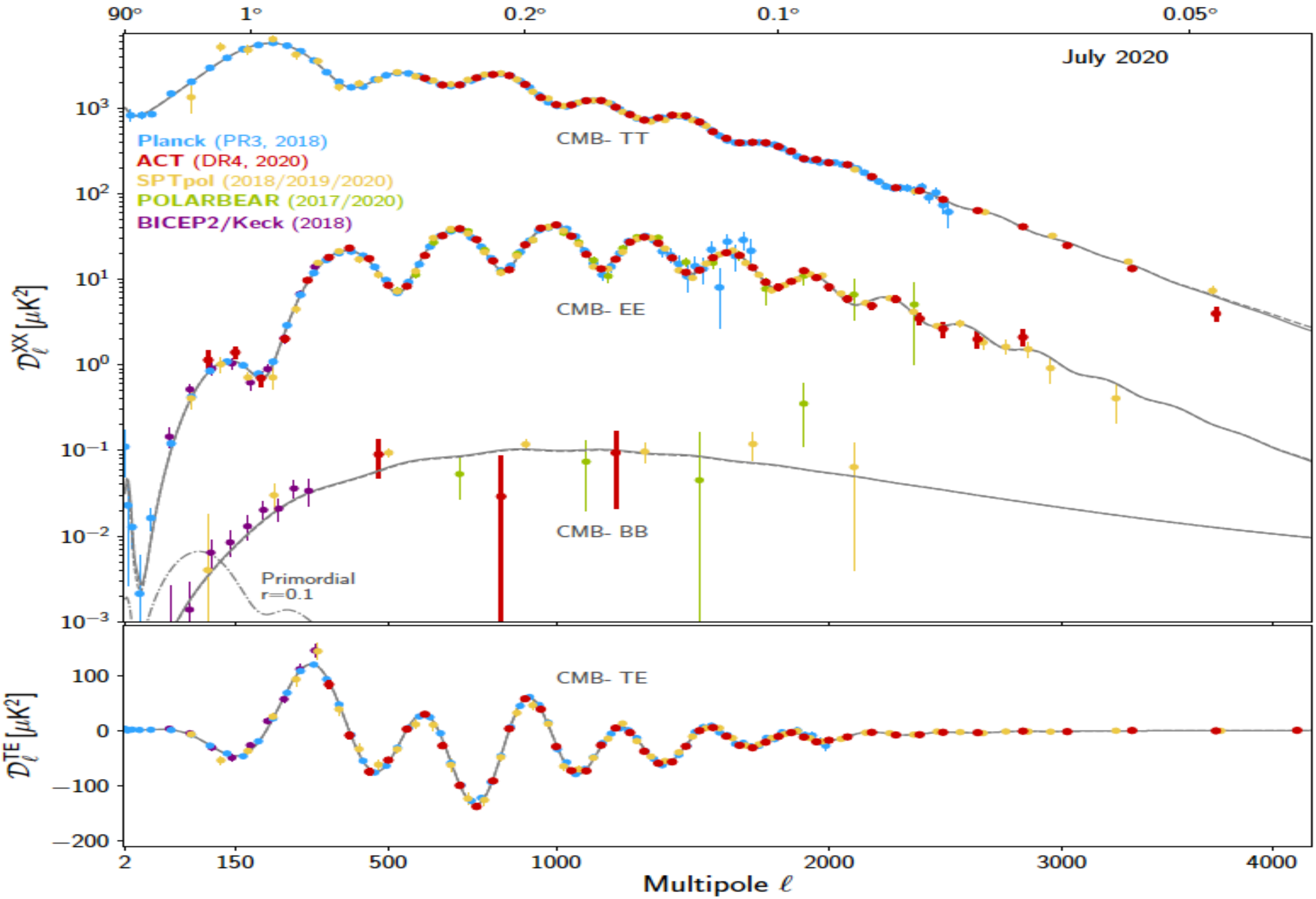

Planck best-fit 6-parameter
ΛCDM model 2018

Density perturbation (scalar)

Spectral index $\mathcal{P}_{\mathcal{R}}(k) = A_s \left(\frac{k}{k_0}\right)^{n_s-1}$

k_0=0.05Mpc^{-1}

Parameter	TT+lowE 68% limits	TE+lowE 68% limits	EE+lowE 68% limits	TT,TE,EE+lowE 68% limits	TT,TE,EE+lowE+lensing 68% limits	TT,TE,EE+lowE+lensing+BAO 68% limits
$\Omega_b h^2$	0.02212 ± 0.00022	0.02249 ± 0.00025	0.0240 ± 0.0012	0.02236 ± 0.00015	0.02237 ± 0.00015	0.02242 ± 0.00014
$\Omega_c h^2$	0.1206 ± 0.0021	0.1177 ± 0.0020	0.1158 ± 0.0046	0.1202 ± 0.0014	0.1200 ± 0.0012	0.11933 ± 0.00091
$100\theta_{MC}$	1.04077 ± 0.00047	1.04139 ± 0.00049	1.03999 ± 0.00089	1.04090 ± 0.00031	1.04092 ± 0.00031	1.04101 ± 0.00029
τ	0.0522 ± 0.0080	0.0496 ± 0.0085	0.0527 ± 0.0090	$0.0544^{+0.0070}_{-0.0081}$	0.0544 ± 0.0073	0.0561 ± 0.0071
$\ln(10^{10} A_s)$	3.040 ± 0.016	$3.018^{+0.020}_{-0.018}$	3.052 ± 0.022	3.045 ± 0.016	3.044 ± 0.014	3.047 ± 0.014
n_s	0.9626 ± 0.0057	0.967 ± 0.011	0.980 ± 0.015	0.9649 ± 0.0044	0.9649 ± 0.0042	0.9665 ± 0.0038
z_{re}	7.50 ± 0.82	$7.11^{+0.91}_{-0.75}$	$7.10^{+0.87}_{-0.73}$	7.68 ± 0.79	7.67 ± 0.73	7.82 ± 0.71

ΛCDM model + 1-parameter extension

Spectral index $\mathcal{P}_{\mathcal{R}}(k) = A_s \left(\frac{k}{k_0}\right)^{n_s - 1}$

r = Tensor/Scalar
= $P_h(k)/P_R(k)$ at k=0.002 Mpc^{-1}

Planck best-fit 7-parameter 2018

Parameter	TT+lowE	TT, TE, EE+lowE	TT, TE, EE+lowE+lensing	TT, TE, EE+lowE+lensing+BAO
Ω_K	$-0.056^{+0.044}_{-0.050}$	$-0.044^{+0.033}_{-0.034}$	$-0.011^{+0.013}_{-0.012}$	$0.0007^{+0.0037}_{-0.0037}$
Σm_ν [eV]	< 0.537	< 0.257	< 0.241	< 0.120
$N_{\rm eff}$	$3.00^{+0.57}_{-0.53}$	$2.92^{+0.36}_{-0.37}$	$2.89^{+0.36}_{-0.38}$	$2.99^{+0.34}_{-0.33}$
$Y_{\rm P}$	$0.246^{+0.039}_{-0.041}$	$0.240^{+0.024}_{-0.025}$	$0.239^{+0.024}_{-0.025}$	$0.242^{+0.023}_{-0.024}$
$dn_s/d\ln k$	$-0.004^{+0.015}_{-0.015}$	$-0.006^{+0.013}_{-0.013}$	$-0.005^{+0.013}_{-0.013}$	$-0.004^{+0.013}_{-0.013}$
$r_{0.002}$	< 0.102	< 0.107	< 0.101	< 0.106
w_0	$-1.56^{+0.60}_{-0.48}$	$-1.58^{+0.52}_{-0.41}$	$-1.57^{+0.50}_{-0.40}$	$-1.04^{+0.10}_{-0.10}$

Joint Planck+WMAP+BICEP/Keck Array constraint 2021
$r_{0.05} < 0.036$ at 95% c.l.

CMB constraints on narrow-peak GWB

Namikawa et al. 2019 considered GWB contribution to CMB anisotropy and B-mode polarization measured by Planck and BICEP/Keck Array

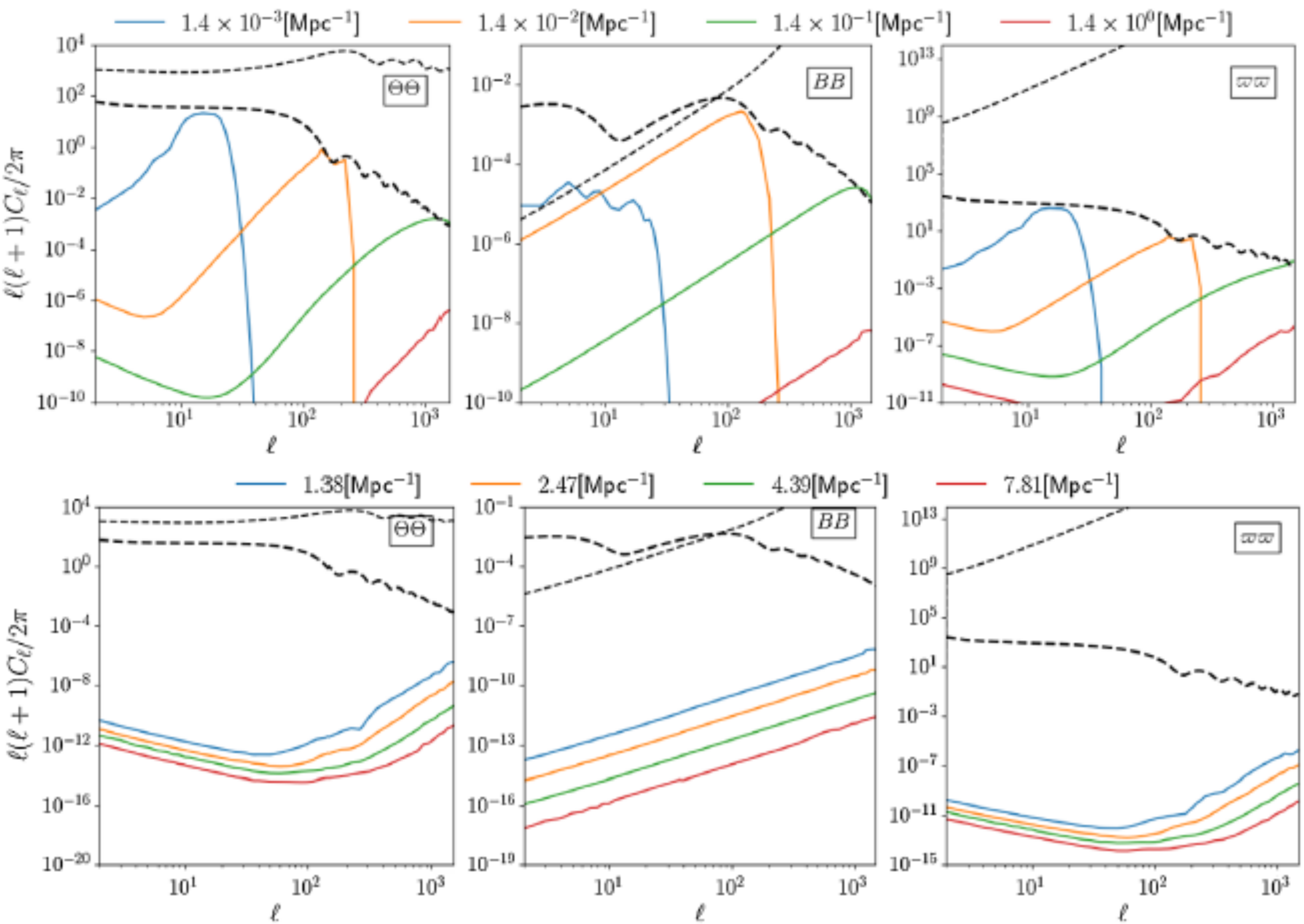

CMB constraints on narrow-peak GWB

Namikawa et al. 2019 considered GWB contribution to CMB anisotropy and B-mode polarization measured by Planck and BICEP/Keck Array (l<2000)

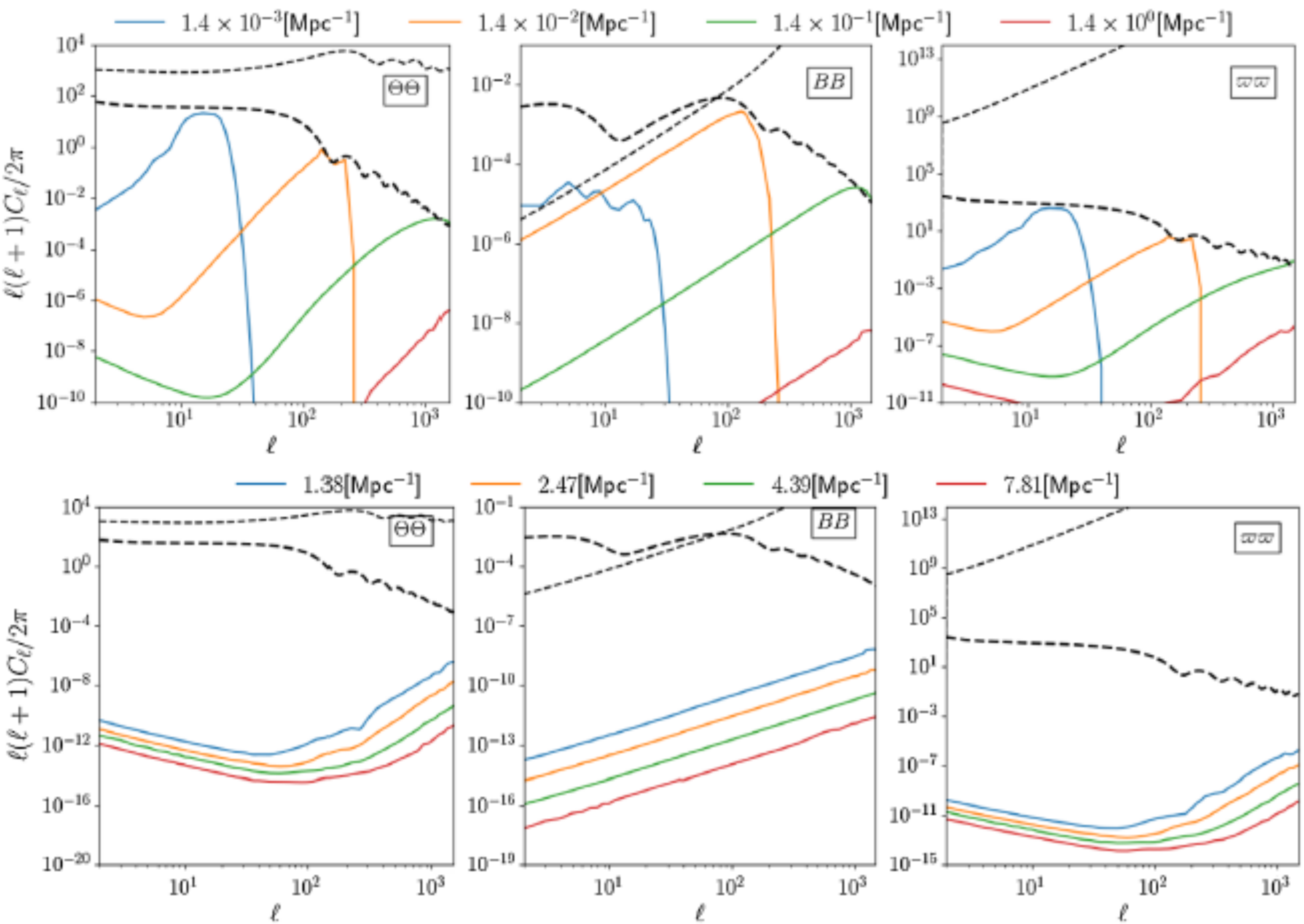

CMB constraints on narrow-peak GWB

Ng 2021 used small-scale temperature anisotropies measured by ACT and SPT (l=3000-10^4) to set an upper limits on GWB

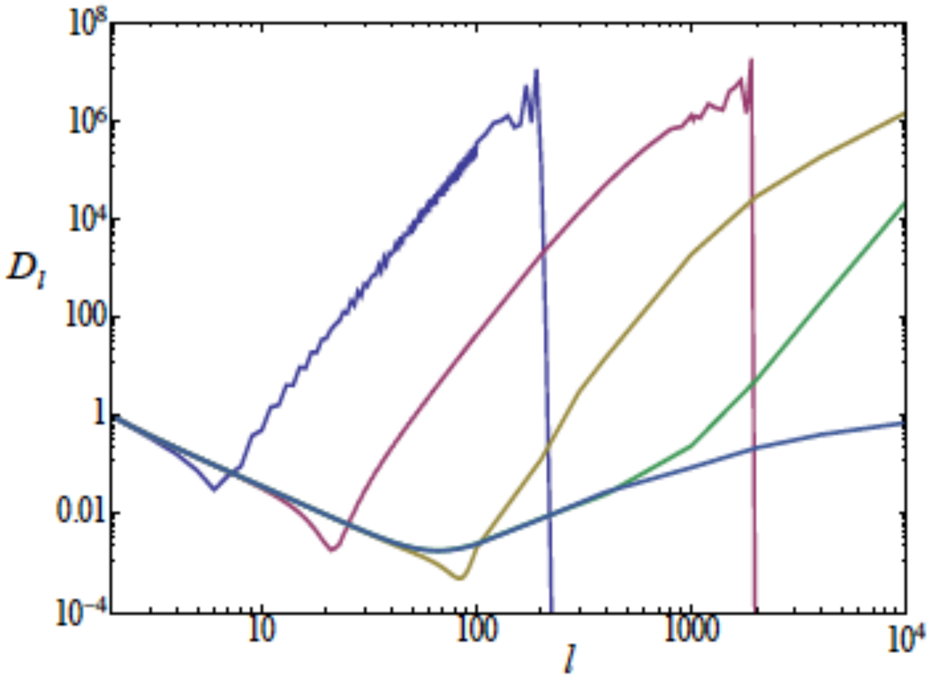

Sachs-Wolfe effect from GWs

$$C_l \simeq \frac{1}{2\pi}(l+2)(l+1)l(l-1) \times \Delta \ln k_* \left| \int_{\eta_1}^{\eta_0} d\eta \frac{dh(k_*\eta)}{d\eta} \frac{j_l[k_*(\eta_0-\eta)]}{k_*^2(\eta_0-\eta)^2} \right|^2$$

FIG. 1. CMB temperature anisotropy power spectra induced by narrow spectra of gravitational waves centered at wavelengths of $k_* = 0.014$, 0.14, 1.4, 14, and 140 Mpc^{-1}, denoted by five solid curves from left to right, respectively. We have defined $D_l \equiv l(l+1)C_l(2\pi M_p^2\eta_0^4)/(M_*^2\eta_*^4)$, where C_l is given by Eq. (21).

Current Upper Bounds

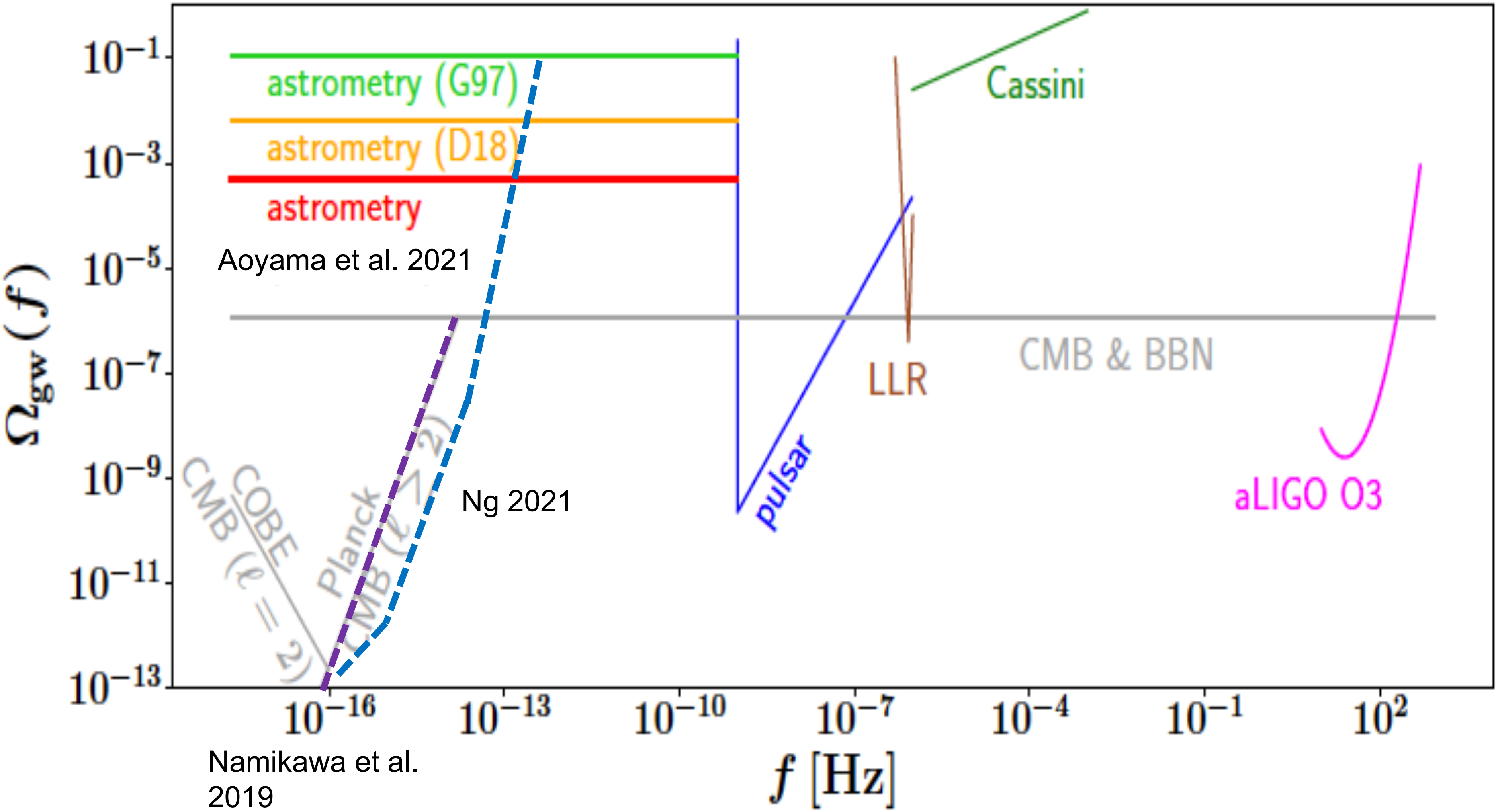

CMB&BBN – extra degrees of freedom
Cassini+LLR – radar launching

CMB – anisotropy + B-mode polarization
aLIGO – direct detection of wave strain
Pulsar – Shapiro time delay
Astrometry – gravitational lensing effect

GW detection in LIGO-Virgo-KAGRA

The method adopted in current GW experiments for detecting SGWB is to correlate responses of different detectors to the GW strain amplitude. This allows us to filter out detector noises and obtain a large signal-to-noise ratio [4]. Let $h(\vec{x})$ be the response of a detector located at $\vec{x}$ with a pair of arms d_{ij}; then, we have

$$h(\vec{x}) \equiv d^{ij} h_{ij}(\vec{x}) = \sum_{\lambda=+,\times} \int \frac{d^3\vec{k}}{(2\pi)^{\frac{3}{2}}} h_\lambda(\vec{k}) F^\lambda(\hat{k}) e^{i\vec{k}\cdot\vec{x}}, \tag{6}$$

where $F^\lambda = d^{ij}\epsilon^\lambda_{ij}(\hat{k})$ is the beam-pattern function. Hence, using Eq. (3) the response correlation between two detectors a and b, located at $\vec{x}_a = \vec{x} + \vec{r}/2$ and $\vec{x}_b = \vec{x} - \vec{r}/2$ respectively, is given by

$$\langle h_a(\vec{x}_a) h_b(\vec{x}_b) \rangle = \sum_{\lambda=+,\times} \int \frac{d^3\vec{k}}{(2\pi)^3} P_h(k) F^\lambda_a(\hat{k}) F^\lambda_b(\hat{k}) e^{i\vec{k}\cdot\vec{r}}, \tag{7}$$

GW power spectrum

$$P_h(k) \equiv (2\pi^2/k^3)\mathcal{P}_h(k)$$

Current Pulsar Timing Arrays (PTAs)

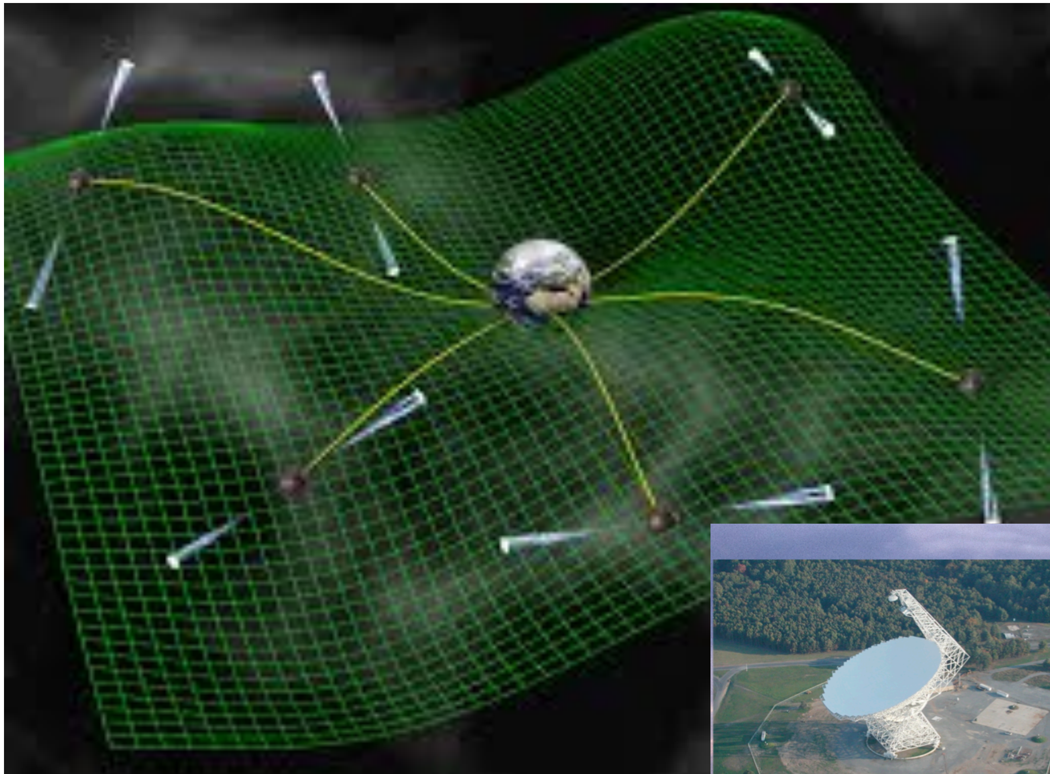

Nano-Hz GWs cause small correlated changes to the times of arrival of radio pulses from millisecond pulsars (MSPs)

International Pulsar Timing Arrays

Pulsar Timing – MSPs are precise clocks

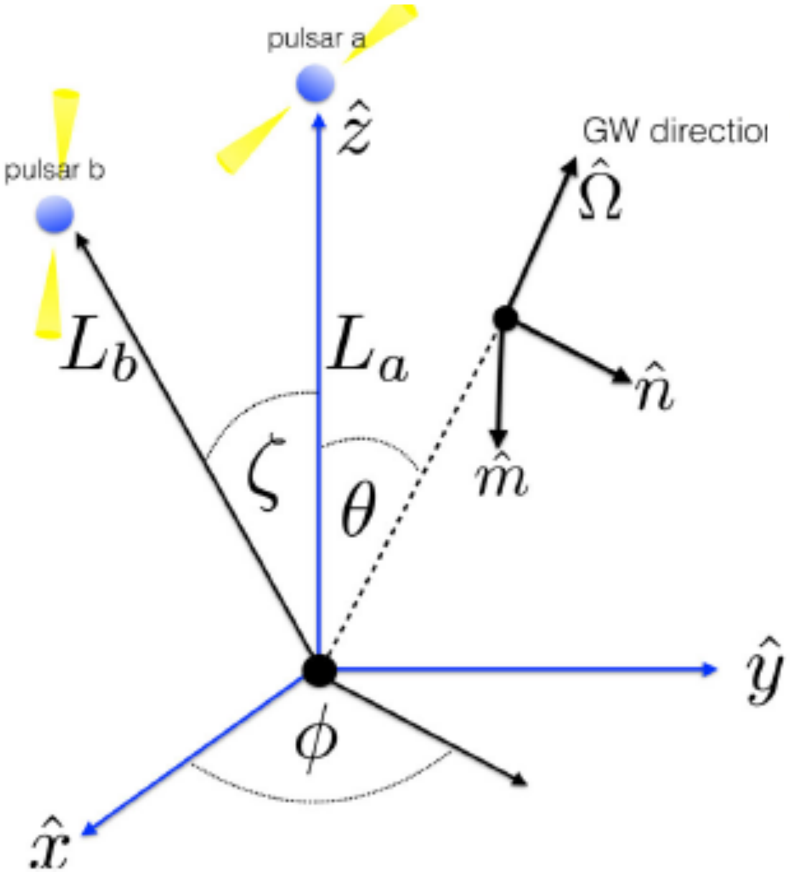

$$z(t,\hat{\Omega}) \equiv \frac{\nu(t)-\nu_0}{\nu_0} = \frac{1}{2}\frac{\hat{p}^i\hat{p}^j}{1+\hat{\Omega}\cdot\hat{p}}\Delta h_{ij}(t,\hat{\Omega}),$$

Shapiro time delay

$$\Delta h_{ij}(t,\hat{\Omega}) \equiv h_{ij}(t,\hat{\Omega}) - h_{ij}(t_{\rm p},\hat{\Omega})$$

$$z(t) = \int d\hat{\Omega} z(t,\hat{\Omega})$$

pulsar residual $$r(t) = \int^t dt' z(t')$$

detector tensor
$d^{ij} = p^i p^j$

$$\langle r_a^*(t_j) r_b(t_k)\rangle = \left\langle \int^{t_j} dt' \int^{t_k} dt'' z_a^*(t') z_b(t'')\right\rangle$$

$$\langle r_a^*(t_j) r_b(t_k)\rangle = \int^{t_j} dt' \int^{t_k} dt'' \int_{-\infty}^{+\infty} df\, e^{-i2\pi f(t'-t'')} H(f)^{(ab)}\Gamma(f)$$

$$\langle h_A^*(f,\hat{\Omega}) h_{A'}(f',\hat{\Omega}')\rangle = \delta^2(\hat{\Omega},\hat{\Omega}')\delta_{AA'}\delta(f-f')H(f)P(\hat{\Omega})$$

Overlap Reduction Function

$$^{(ab)}\Gamma(f) \equiv \int d\hat{\Omega}\, P(\hat{\Omega})\kappa_{ab}(f,\hat{\Omega})\left[\sum_A F_a^A(\hat{\Omega})F_b^A(\hat{\Omega})\right],$$

$$\kappa_{ab}(f,\hat{\Omega}) \equiv [1 - e^{i2\pi f L_a(1+\hat{\Omega}\cdot\hat{p}_a)}][1 - e^{-i2\pi f L_b(1+\hat{\Omega}\cdot\hat{p}_b)}], \qquad F^A(\hat{\Omega}) = \left[\frac{1}{2}\frac{\hat{p}^i\hat{p}^j}{1+\hat{\Omega}\cdot\hat{p}} e_{ij}^A(\hat{\Omega})\right]$$

Earth term

pulsar term $fL >> 1$

(a)

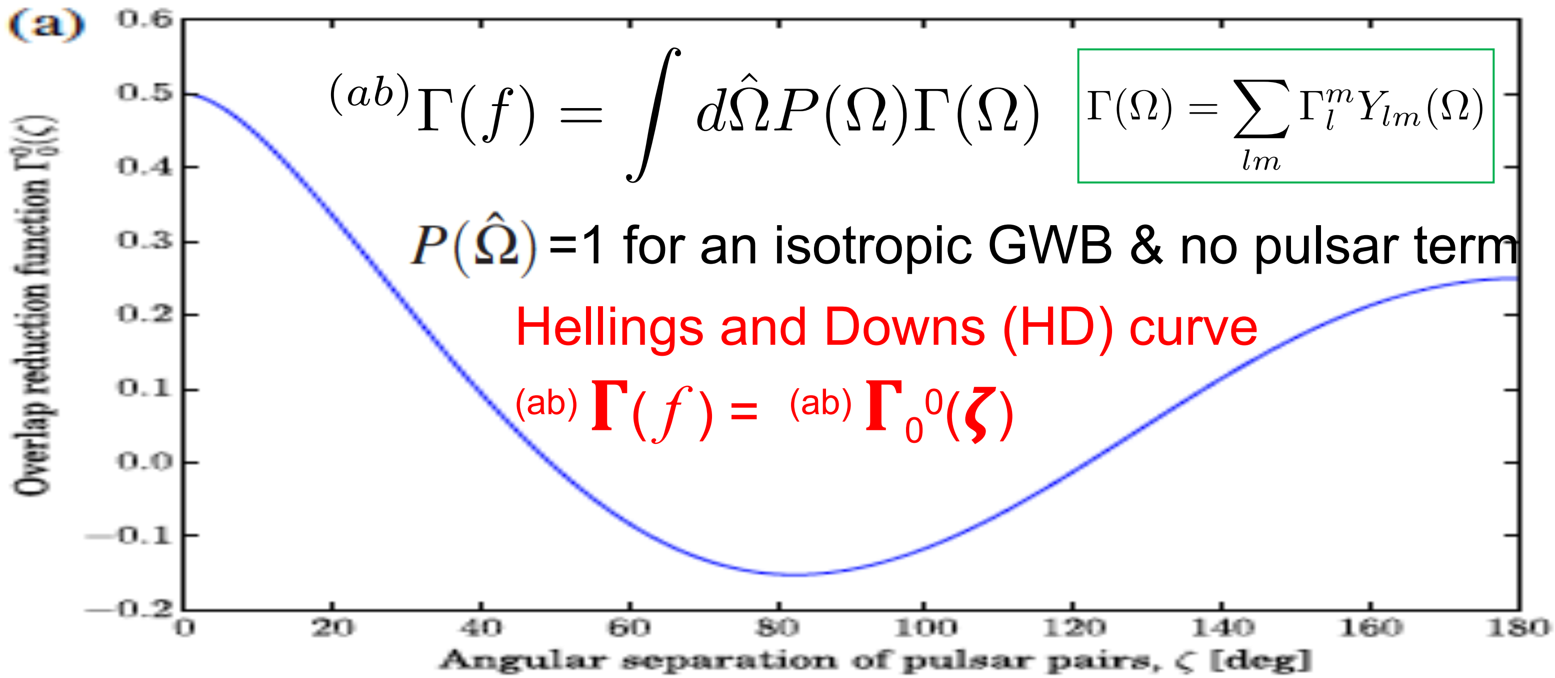

Signal

$$h_c(f) = A_{\rm GWB}\left(\frac{f}{f_{\rm yr}}\right)^{\alpha} \qquad \alpha = -2/3 \text{ for a population of inspiraling SMBHBs}$$

Pulsar residual

$$\langle r_a^*(t_j) r_b(t_k)\rangle = S_{ab}(f) = \Gamma_{ab}\frac{{A_{\rm GWB}}^2}{12\pi^2}\left(\frac{f}{f_{\rm yr}}\right)^{-\gamma} f_{\rm yr}^{-3}. \qquad \boxed{\gamma = 3 - 2\alpha}$$

- Monopolar ORF $\Gamma_{ab}=1$ (*due to clock error*)
- Dipolar ORF $\Gamma_{ab}= \cos\zeta$ (*due to error in solar system ephemeris*)
- Quadupolar ORF Γ_{ab} = HD curve (*genuine GWB signal*)

Noise

white noises (instrumental) + pulsar intrinsic red noise (including pulsar spin noise, pulsar profile changes, dispersion measure variations,…)

$$N_{aa}(f) = {A_{red}}^2 \,(f / f_{yr})^{-\gamma}\, {f_{yr}}^{-3}$$

NANOGrav Physics Frontiers Center

North American Nanohertz Observatory for Gravitational Waves

North American Nanohertz Observatory for Gravitational Waves

A National Science Foundation Physics Frontiers Center

The NANOGrav 12.5-year Data Set: Search For An Isotropic Stochastic Gravitational-Wave Background arXiv:2009.04496 9 Sep 2020

We search for an isotropic stochastic gravitational-wave background (GWB) in the 12.5-year pulsar timing data set collected by the North American Nanohertz Observatory for Gravitational Waves (NANOGrav). Our analysis finds strong evidence of a stochastic process, modeled as a power-law, with common amplitude and spectral slope across pulsars. The Bayesian posterior of the amplitude for a $f^{-2/3}$ power-law spectrum, expressed as characteristic GW strain, has median 1.92×10^{-15} and 5%–95% quantiles of 1.37–2.67×10^{-15} at a reference frequency of $f_{\rm yr} = 1\ {\rm yr}^{-1}$. The Bayes factor in favor of the common-spectrum process versus independent red-noise processes in each pulsar exceeds 10,000. However, we find no statistically significant evidence that this process has quadrupolar spatial correlations, which we would consider necessary to claim a GWB detection consistent with General Relativity. We find that the process has neither monopolar nor dipolar correlations, which may arise from, for example, reference clock or solar-system ephemeris systematics, respectively. The amplitude posterior has significant support above previously reported upper limits; we explain this in terms of the Bayesian priors assumed for intrinsic pulsar red noise. We examine potential implications for the supermassive black hole binary population under the hypothesis that the signal is indeed astrophysical in nature.

$$\boxed{h_c = A = 1.92\times 10^{-15}}$$

$$\boxed{\Omega_{\rm GW} h^2 = \frac{2\pi^2}{3} h_c^2 \left(\frac{f_{\rm yr}}{100\,{\rm km\,s^{-1}Mpc^{-1}}}\right)^2 \simeq 2.3\times 10^{-9}}$$

Common-spectrum Process supported by

PPTA arXiv:2107.12112

EPTA arXiv:2110.13184

IPTA arXiv:2201.03980

The NANOGrav 12.5 year data set: 45 MSPs

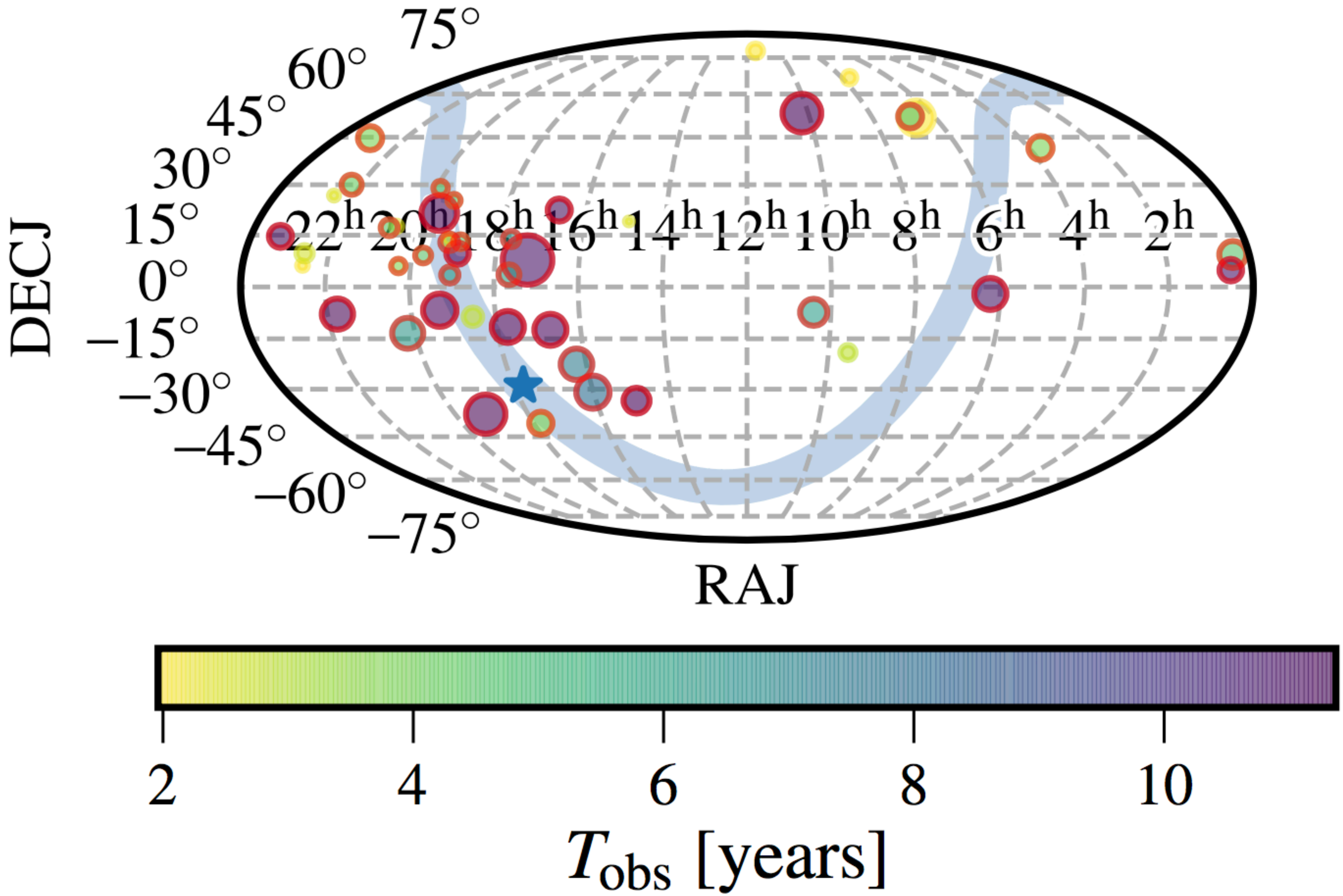

Image: sky map of NANOGrav pulsars in the 11-yr data set

common-spectrum process across MSPs $S_{aa}(f)$

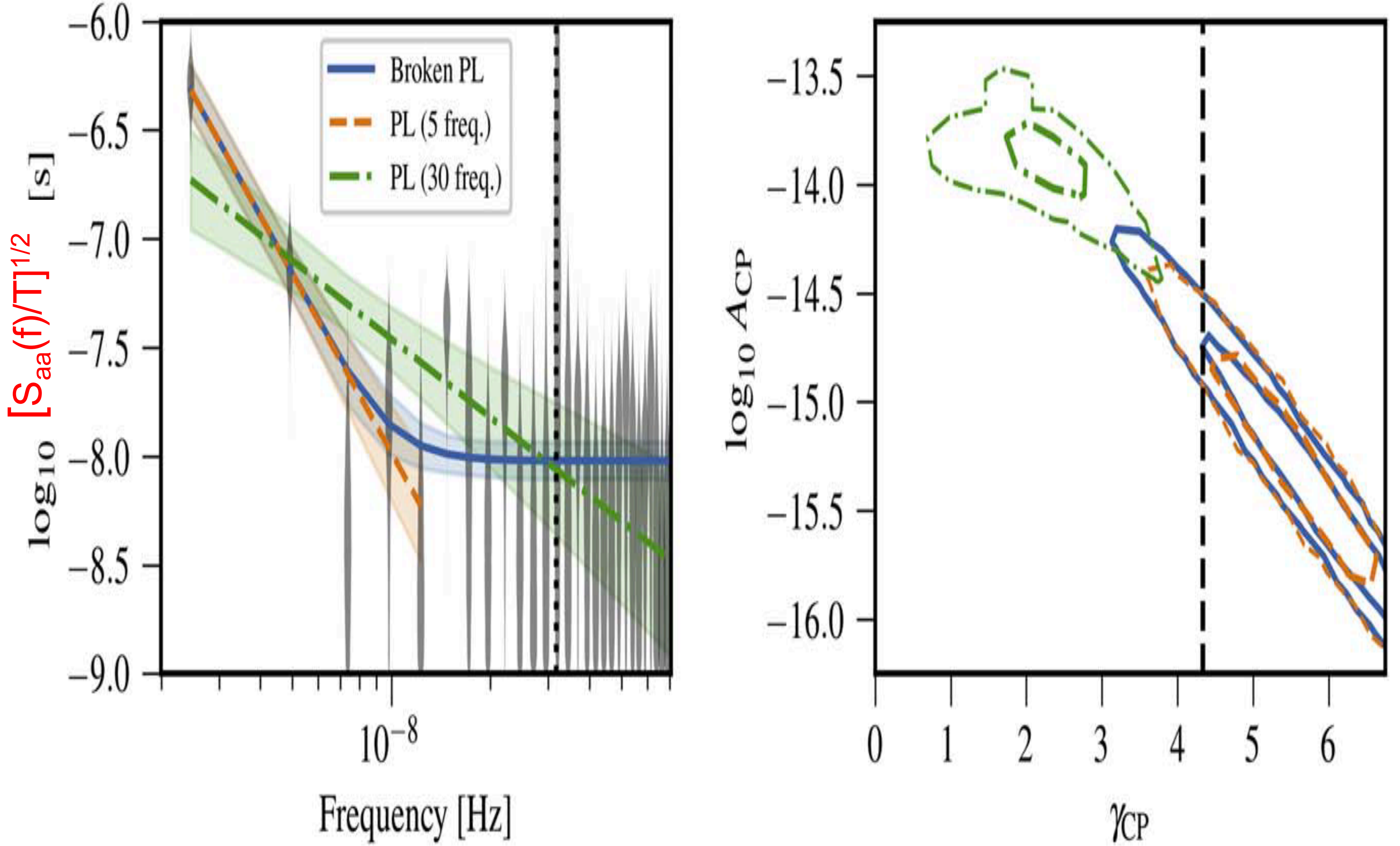

Spatial correlation $S_{ab}(f)$

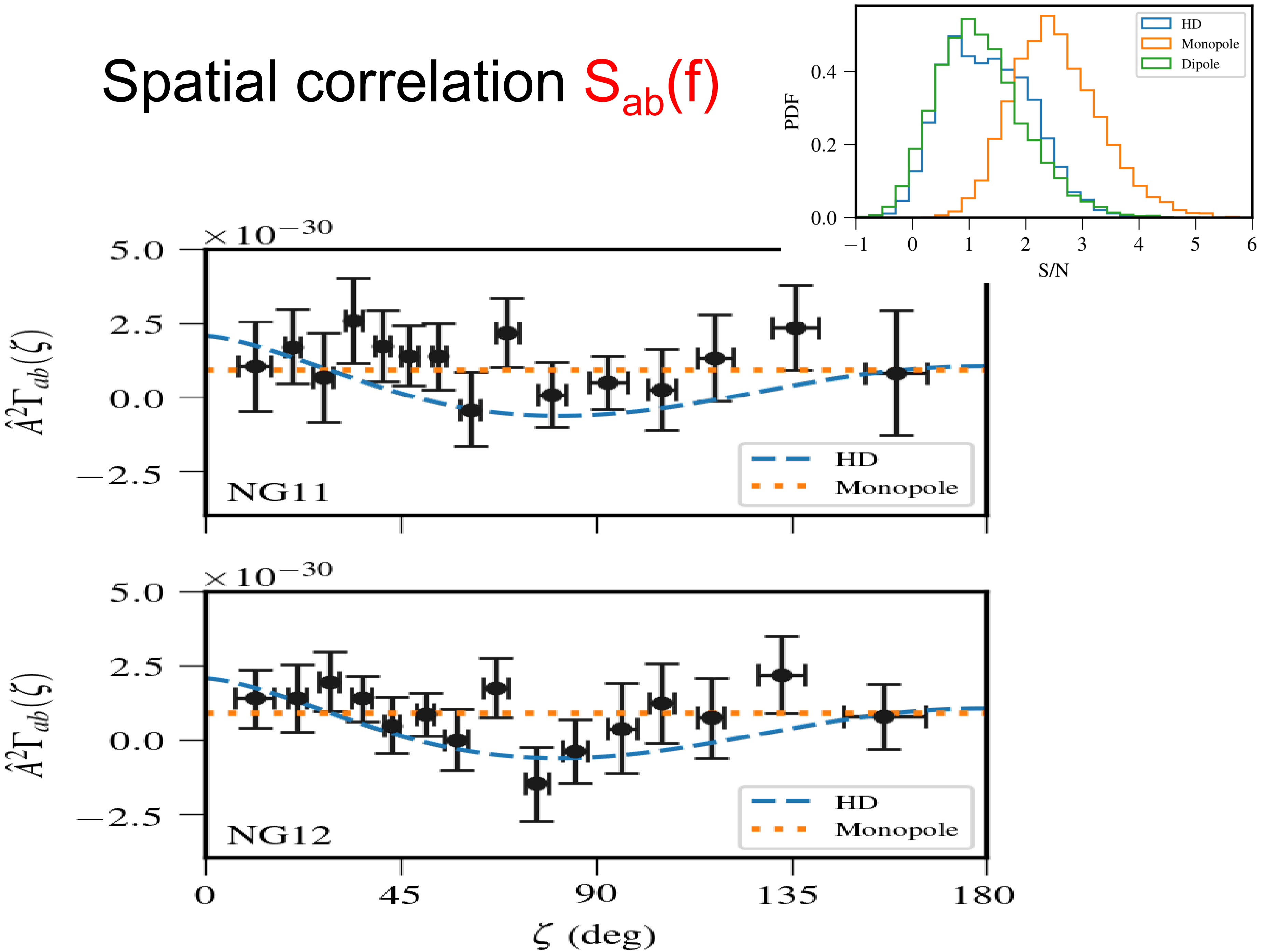

Future SKA will observe thousands of millisecond pulsars

Astrometric observation of SGWB

Astrometry is another indirect search for a SGWB using precise measurements of the positions, distances, and motions of celestial objects [17–25]. The subject has recently attracted a lot of attention due to high-precision astrometric data made by the *Gaia* space optical observatory [26]. A SGWB will induce fluctuations of the apparent angular positions of stars, which are independent of the star distances and correlated over the sky [17, 19, 20]. The rms fluctuation can be estimated as given by the GW characteristic strain amplitude,

$$\delta_{\rm rms} \sim h_c(f), \quad \text{with} \quad \Omega_{\rm GW} = \frac{2\pi^2}{3H_0^2} h_c^2 f^2 \,. \tag{1}$$

This leads to a rms angular velocity,

$$\omega_{\rm rms} \sim f\delta_{\rm rms} \sim H_0\sqrt{\Omega_{\rm GW}}\,, \tag{2}$$

which is constant for a flat spectral energy density.

Suppose we monitor the positions of N stars in an observation with an angular resolution of $\Delta\theta$ over a time period of T. Then, the sensitivity of detecting an angular motion of a star will be $\Delta\theta/(T\sqrt{N})$ for a frequency $f < 1/T$, which means that we can detect a SGWB with [20]

$$\Omega_{\rm GW}(f < 1/T) \sim \left(\frac{\Delta\theta}{T}\right)^2 \frac{1}{NH_0^2} \,. \tag{3}$$

$\Delta\boldsymbol{\theta}\sim\boldsymbol{\lambda}/D$

$\boldsymbol{\lambda}$ observing wavelength

D telescope size

Very Long Baseline Interferometry (LVBI)

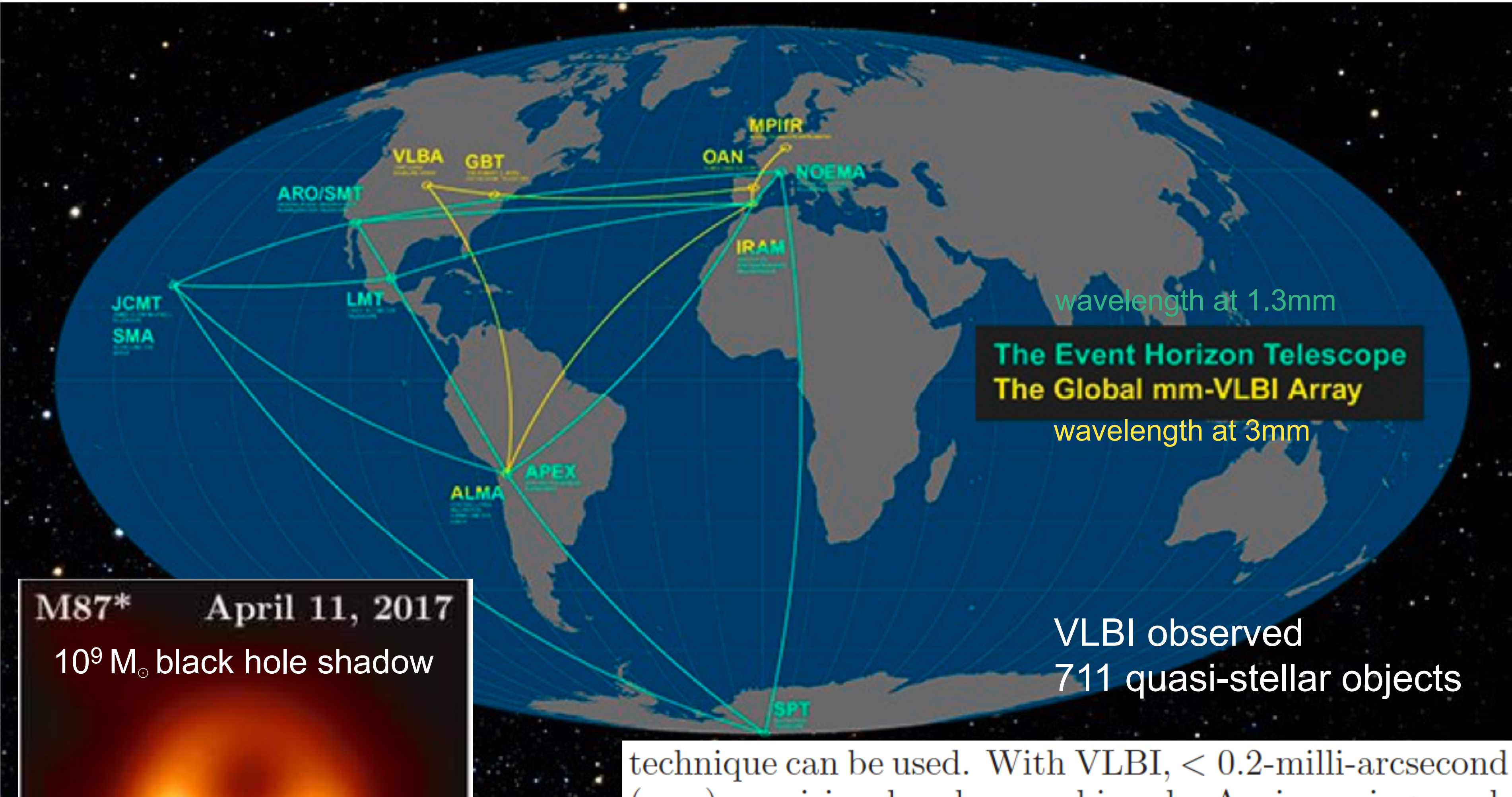

technique can be used. With VLBI, < 0.2-milli-arcsecond (mas) precision has been achieved. A pioneering work of this technique is Gwinn et al. (1997) [10], hereafter G97. Darling et al. (2018) [11], hereafter D18, measure proper motions of 711 objects with the VLBI and set a upper limit on low frequency GWs, $\Omega_{\rm gw} < 0.64 \times 10^{-2}$ for $f < 10^{-9}$ Hz. While the VLBI technique is successful, *Gaia* space optical telescope (2013-2022) for astrometry: measuring the positions, distances and motions of a billion stars with micro arcsecond precision.

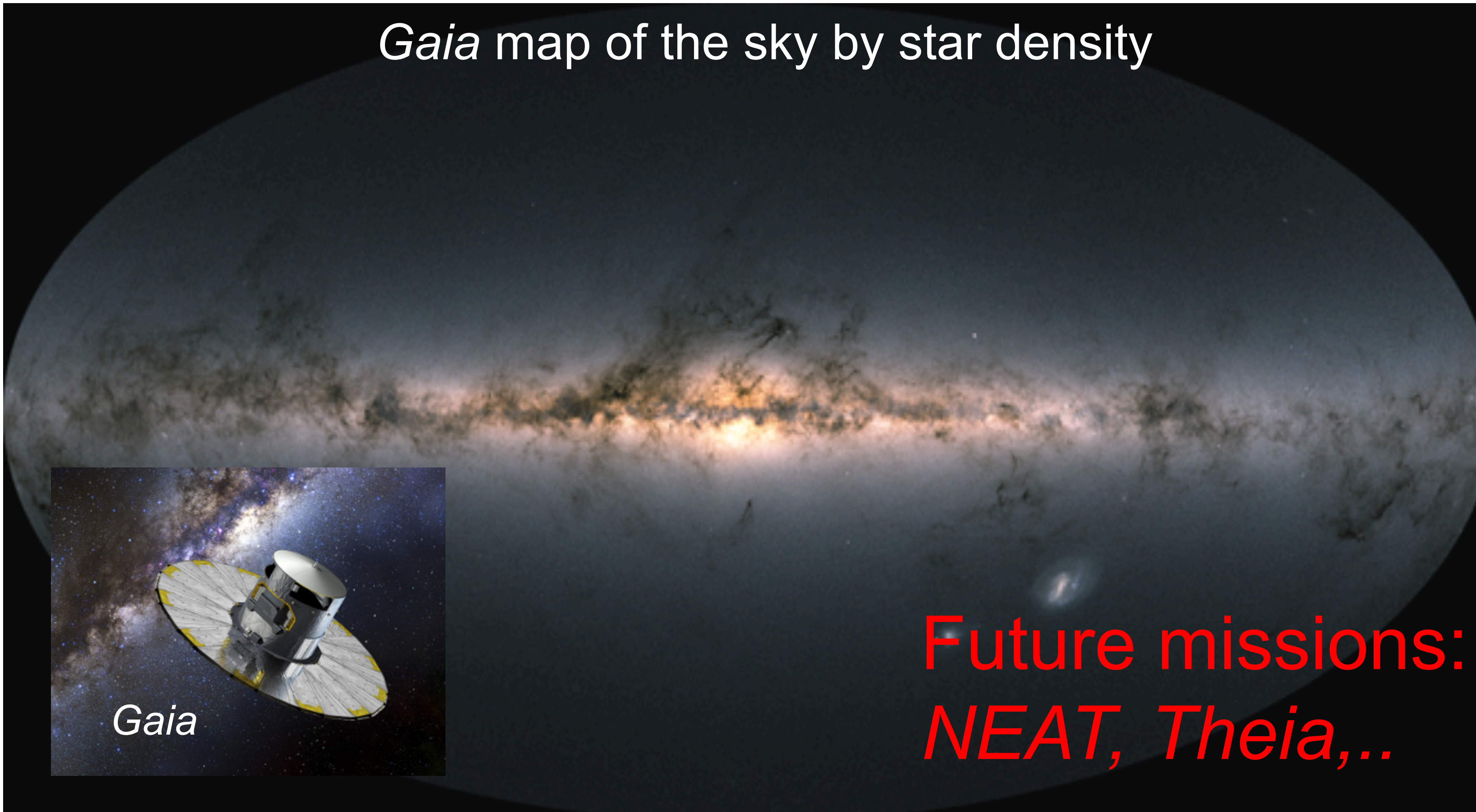

Gaia 400,894 QSO constraint on the energy density of low-frequency gravitational waves

Shohei Aoyama, Daisuke Yamauchi, Maresuke Shiraishi, Masami Ouchi (May 9, 2021)

e-Print: 2105.04039 [gr-qc]

Low frequency gravitational waves (GWs) are keys to understanding cosmological inflation and super massive blackhole (SMBH) formation via blackhole mergers, while it is difficult to identify the low frequency GWs with ground-based GW experiments such as the advanced LIGO (aLIGO) and VIRGO due to the seismic noise. Although quasi-stellar object (QSO) proper motions produced by the low frequency GWs are measured by pioneering studies of very long baseline interferometry (VLBI) observations with good positional accuracy, the low frequency GWs are not strongly constrained by the small statistics with 711 QSOs (Darling et al. 2018). Here we present the proper motion field map of 400,894 QSOs of the Sloan Digital Sky Survey (SDSS) with optical *Gaia* EDR3 proper motion measurements whose positional accuracy is < 0.4 milli-arcsec comparable with the one of the radio VLBI observations. We obtain the best-fit spherical harmonics with the typical field strength of $\mathcal{O}(0.1)\,\mu$arcsec, and place a tight constraint on the energy density of GWs, $\Omega_{\rm gw} = (0.964 \pm 3.804) \times 10^{-4}$ (95 % confidence level), that is significantly stronger than the one of the previous VLBI study by two orders of magnitude at the low frequency regime of $f < 10^{-9}\,[\mathrm{Hz}] \simeq (30\,\mathrm{yr})^{-1}$ unexplored by the pulsar timing technique. Our upper limit rules out the existence of SMBH binary systems at the distance $r < 400$ kpc from the Earth where the Milky Way center and local group galaxies are included. Demonstrating the limit given by our optical QSO study, we claim that astrometric satellite data including the forthcoming *Gaia* DR5 data with small systematic errors are powerful to constrain low frequency GWs.

Current Upper Bounds

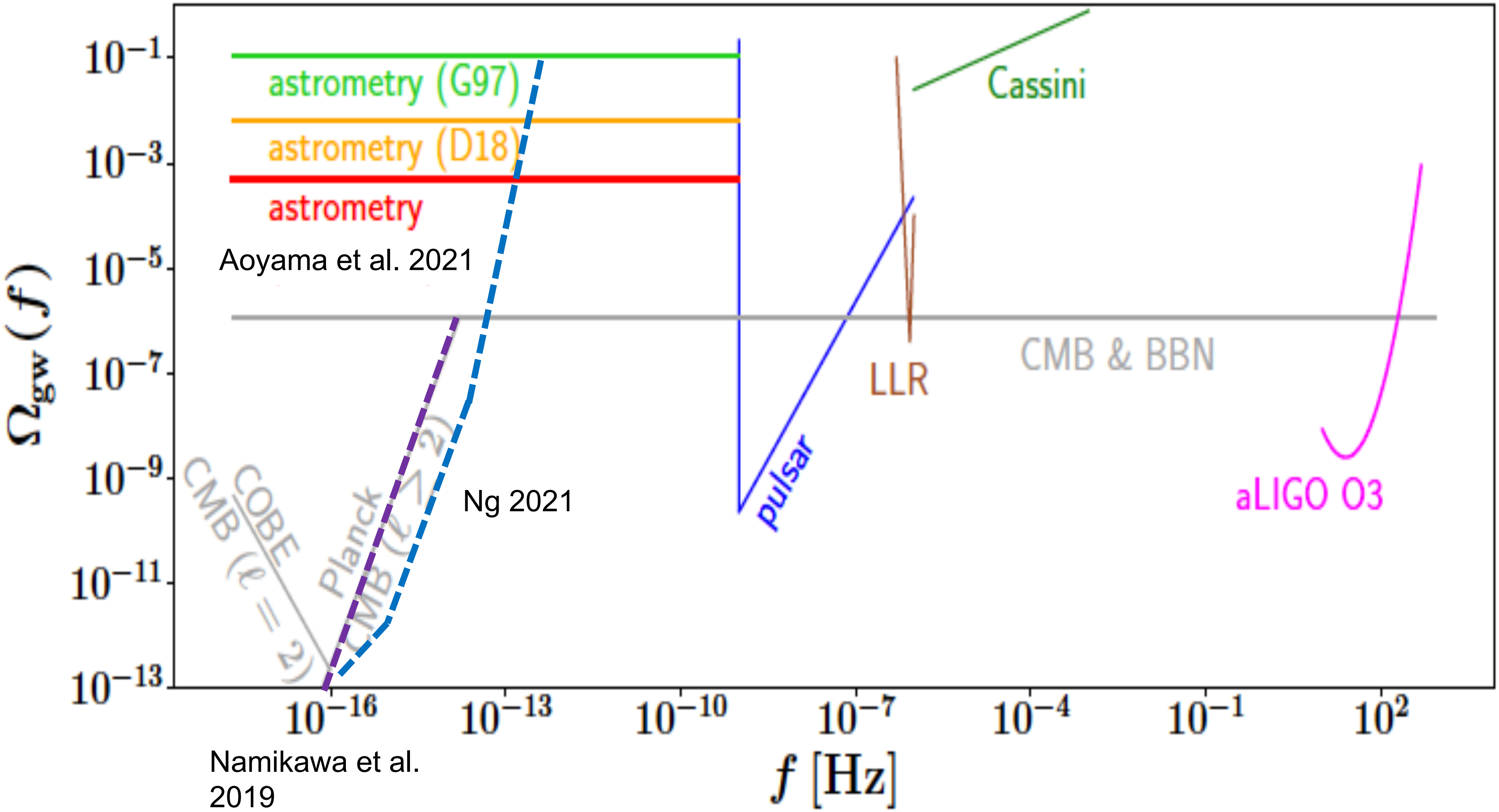

CMB&BBN – extra degrees of freedom
Cassini+LLR – radar launching

CMB – anisotropy + B-mode polarization
aLIGO – direct detection of wave strain
Pulsar – Shapiro time delay
Astrometry – gravitational lensing effect

Future data pipelines

A fast algorithm to generate overlap reduction functions (ORFs - responses of detectors) to polarized GWs

Gravitational Waves

$$h_{ij}(t,\boldsymbol{x}) = \sum_{P=+,\times} \int_{-\infty}^{\infty} df \int_{S^2} d\boldsymbol{n}\, h_P(f,\boldsymbol{n}) e^{2\pi i f(-t+\boldsymbol{n}\cdot\boldsymbol{x})} e_{ij}^P(\boldsymbol{n}). \tag{1}$$

Here, the bases for transverse-traceless tensor $\boldsymbol{e}^P$ ($P = +, \times$) are given as

$$\boldsymbol{e}^+ = \hat{\boldsymbol{e}}_\theta \otimes \hat{\boldsymbol{e}}_\theta - \hat{\boldsymbol{e}}_\phi \otimes \hat{\boldsymbol{e}}_\phi, \qquad \boldsymbol{e}^\times = \hat{\boldsymbol{e}}_\theta \otimes \hat{\boldsymbol{e}}_\phi + \hat{\boldsymbol{e}}_\phi \otimes \hat{\boldsymbol{e}}_\theta,$$

$$\begin{pmatrix} \langle h_+(f,\boldsymbol{n}) h_+^*(f',\boldsymbol{n}')\rangle & \langle h_+(f,\boldsymbol{n}) h_\times^*(f',\boldsymbol{n}')\rangle \\ \langle h_\times(f,\boldsymbol{n}) h_+^*(f',\boldsymbol{n}')\rangle & \langle h_\times(f,\boldsymbol{n}) h_\times^*(f',\boldsymbol{n}')\rangle \end{pmatrix}$$
$$= \frac{1}{2}\delta_{\mathrm{D}}^2(\boldsymbol{n}-\boldsymbol{n}')\delta_{\mathrm{D}}(f-f')$$
$$\times \begin{pmatrix} I(f,\boldsymbol{n}) + Q(f,\boldsymbol{n}) & U(f,\boldsymbol{n}) - iV(f,\boldsymbol{n}) \\ U(f,\boldsymbol{n}) + iV(f,\boldsymbol{n}) & I(f,\boldsymbol{n}) - Q(f,\boldsymbol{n}) \end{pmatrix},$$

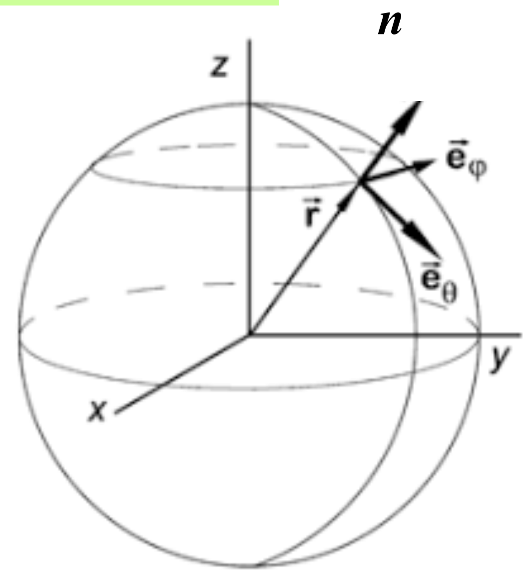

Q= <++> - <xx>
U is the same as in
a frame rotated by **π**/8

$$\boldsymbol{e}^R = \frac{(\boldsymbol{e}^+ + i\boldsymbol{e}^\times)}{\sqrt{2}}, \qquad \boldsymbol{e}^L = \frac{(\boldsymbol{e}^+ - i\boldsymbol{e}^\times)}{\sqrt{2}}$$

$$h_R = \frac{(h_+ - ih_\times)}{\sqrt{2}}, \qquad h_L = \frac{(h_+ + ih_\times)}{\sqrt{2}}$$

$$\begin{pmatrix} \langle h_R(f,\boldsymbol{n}) h_R(f',\boldsymbol{n}')^*\rangle & \langle h_L(f,\boldsymbol{n}) h_R(f',\boldsymbol{n}')^*\rangle \\ \langle h_R(f,\boldsymbol{n}) h_L(f',\boldsymbol{n}')^*\rangle & \langle h_L(f,\boldsymbol{n}) h_L(f',\boldsymbol{n}')^*\rangle \end{pmatrix}$$
$$= \frac{1}{2}\delta_{\mathrm{D}}(\boldsymbol{n}-\boldsymbol{n}')^2\delta_{\mathrm{D}}(f-f')$$
$$\times \begin{pmatrix} I(f,\boldsymbol{n}) + V(f,\boldsymbol{n}) & Q(f,\boldsymbol{n}) - iU(f,\boldsymbol{n}) \\ Q(f,\boldsymbol{n}) + iU(f,\boldsymbol{n}) & I(f,\boldsymbol{n}) - V(f,\boldsymbol{n}) \end{pmatrix}.$$

GWB Anisotropy and Polarization Angular Power Spectra

Decompose the GWB sky into a sum of spherical harmonics:

$$T(\theta,\varphi) = \Sigma_{lm}\ a_{lm}\, Y_{lm}(\theta,\varphi), \quad V(\theta,\varphi) = \Sigma_{lm}\ b_{lm}\, Y_{lm}(\theta,\varphi)$$

$$(Q - iU)(\theta,\varphi) = \Sigma_{lm}\ a_{4,lm}\ {}_{4}Y_{lm}(\theta,\varphi)$$

$$(Q + iU)(\theta,\varphi) = \Sigma_{lm}\ a_{-4,lm}\ {}_{-4}Y_{lm}(\theta,\varphi)$$

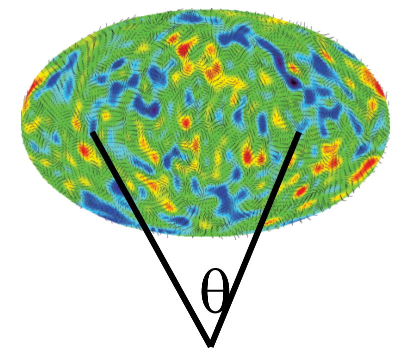

l = 180 degrees/ θ

$C^T_l = \Sigma_m (a^*_{lm}\, a_{lm})$ anisotropy power spectrum

$C^V_l = \Sigma_m (b^*_{lm}\, b_{lm})$ circular polarization power spectrum

$C^E_l = \Sigma_m (a^*_{4,lm}\, a_{4,lm} + a^*_{4,lm}\, a_{-4,lm})$ E-polarization power spectrum

$C^B_l = \Sigma_m (a^*_{4,lm}\, a_{4,lm} - a^*_{4,lm}\, a_{-4,lm})$ B-polarization power spectrum

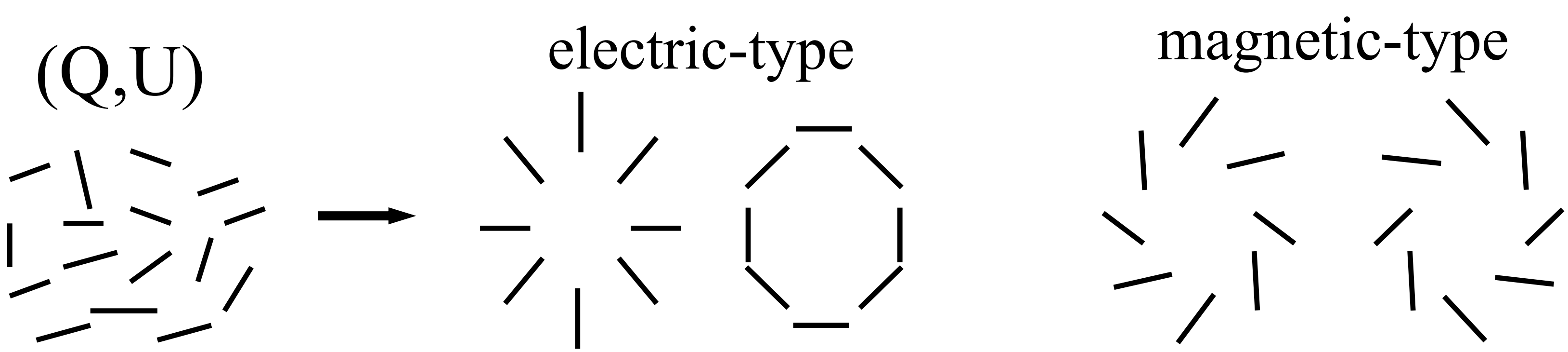

We have developed an efficient tool for generating ORF spherical harmonics $\Gamma_{lm}(f)$ for LIGO-Virgo-KAGRA detector pair

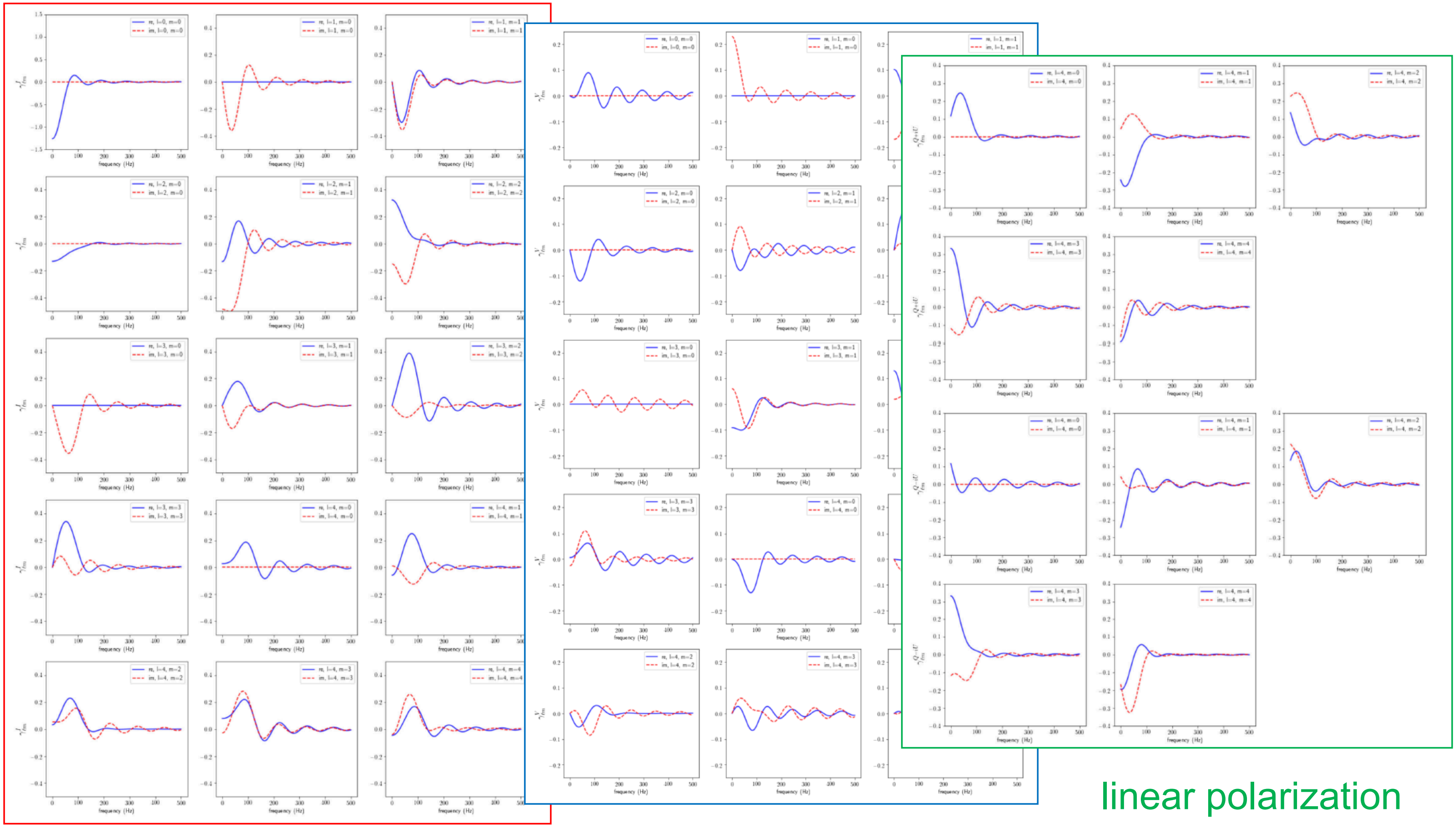

anisotropy

circular polarization

linear polarization

Chu+Liu+Ng 21

Future GW direct experiments

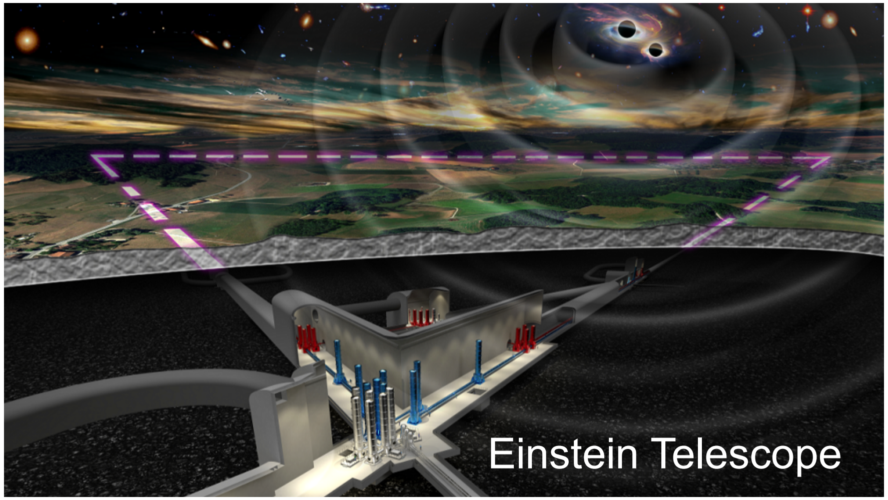

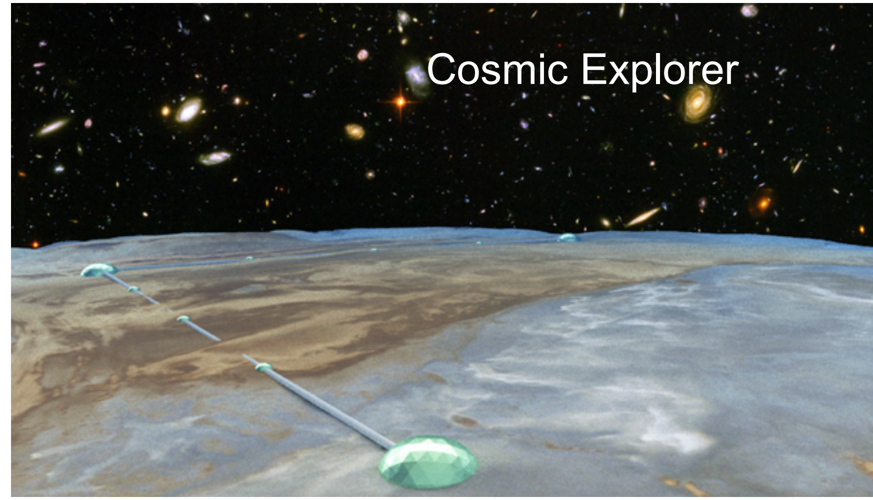

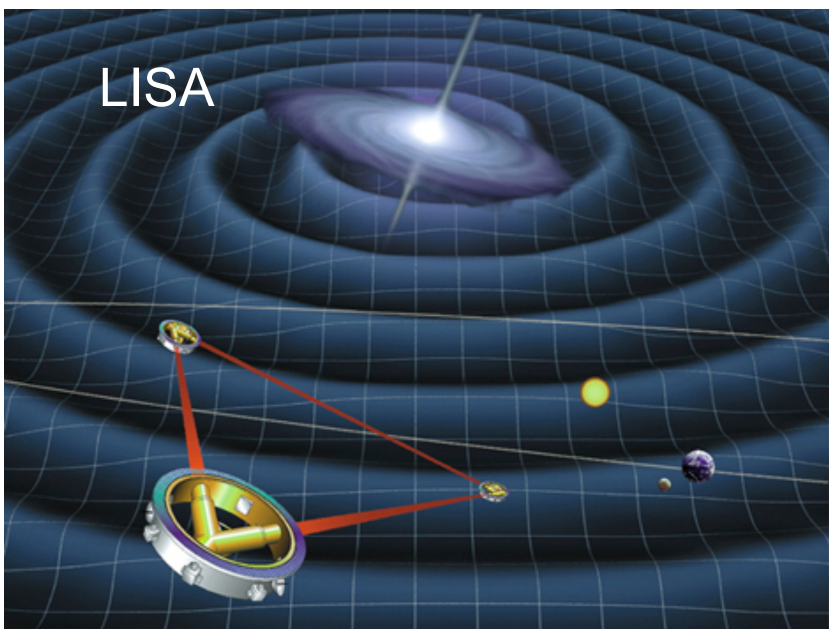

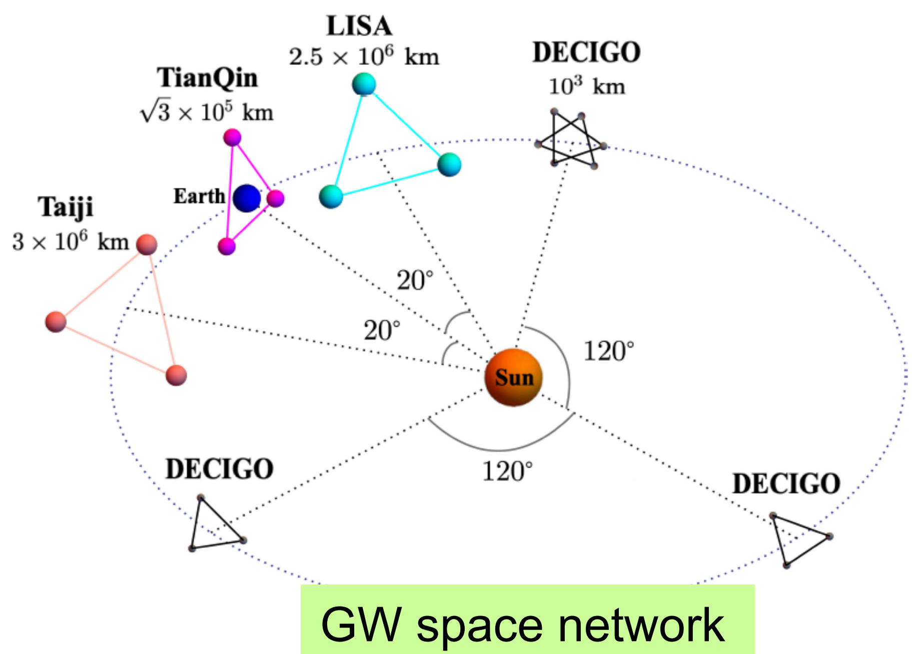

Correlation data live on SO(3) manifold

$$\xi_{ab}(f,\vec{r}) = \int_{-T/2}^{T/2} \mathbf{d}\tau \langle h_a(t_a,\vec{x}_a) h_b^*(t_b,\vec{x}_b)\rangle e^{2\pi i f\tau}$$

$$\xi_{ab}(\alpha,\theta_a,\phi_a) \qquad \vec{x}_a\,(\theta_a,\phi_a)$$

$$T_{mm'm''} = \frac{1}{(2\pi)^3}\int_0^{2\pi} d\alpha d\theta_a d\phi_a \xi_{ab}(\alpha,\theta_a,\phi_a) \times e^{-im\alpha - im'\theta_a - im''\phi_a},$$

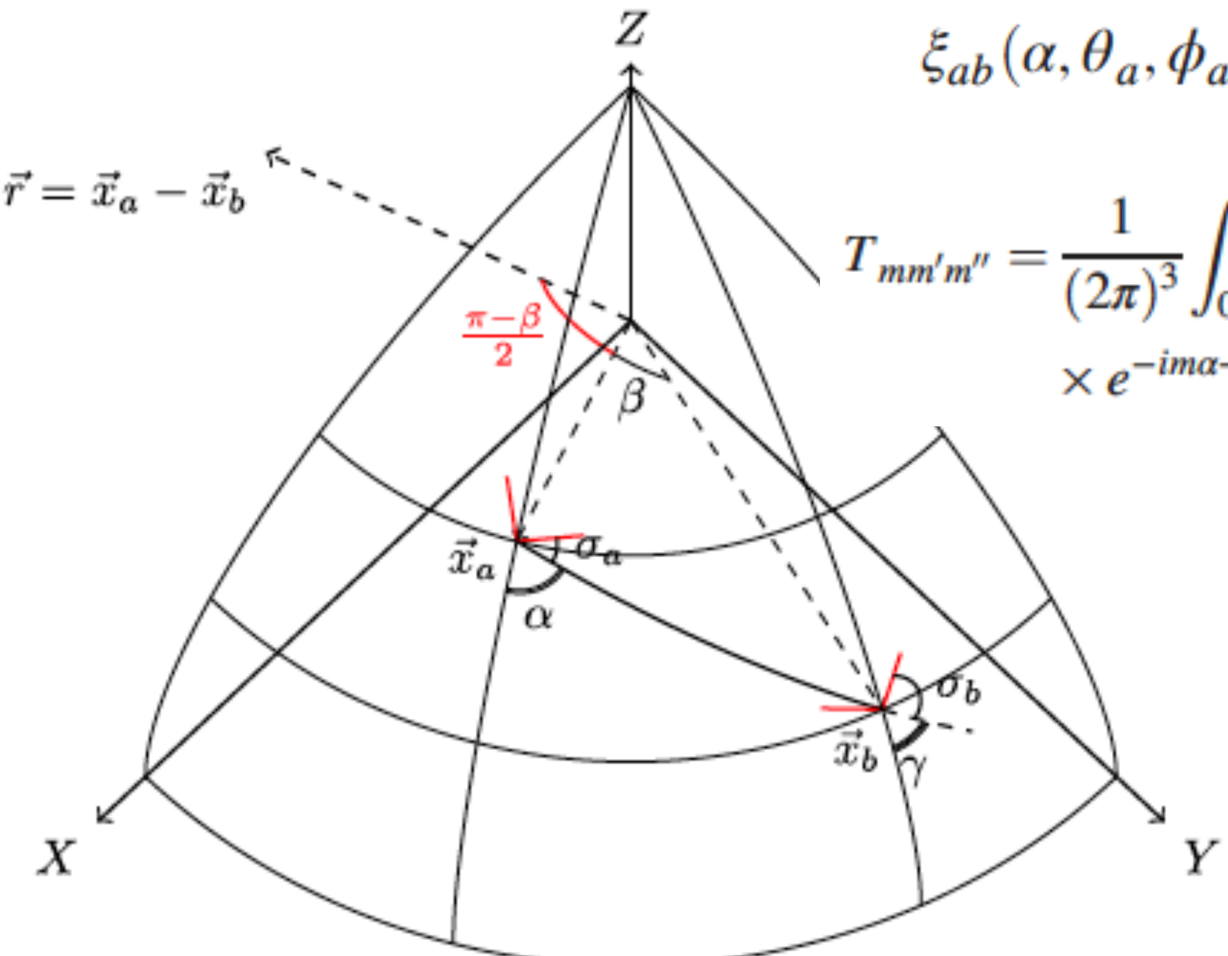

Chu+Liu+Ng 21

We have developed an efficient tool for generating ORF $\Gamma_{lm}(\zeta)$ for any pulsar pair with separation angle ζ

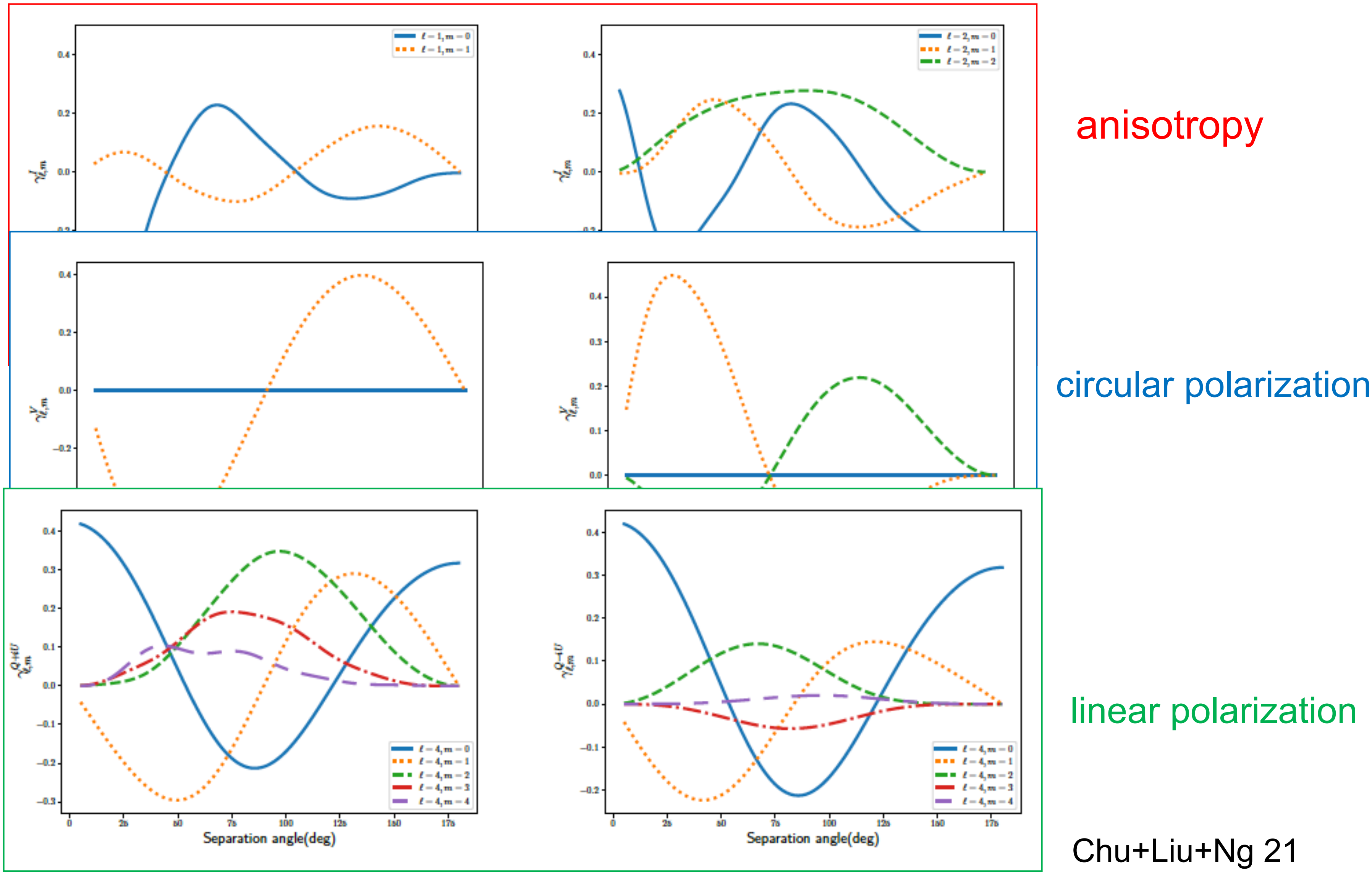

Chu+Liu+Ng 21

Correction to Hellings-Downs curve from the pulsar term

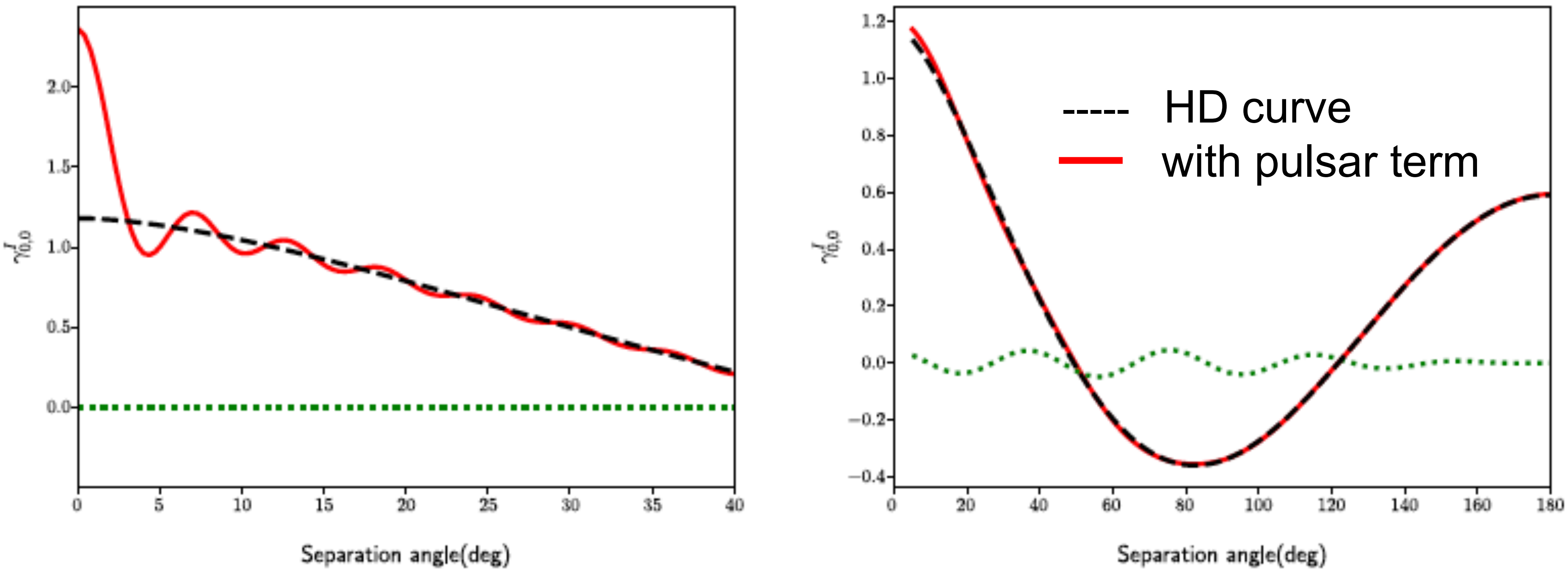

Power spectrum of the pulsar timing residual correlation (l-space)

$$\langle r(t_1)r(t_2)\rangle = \int_0^{t_1} dt' \int_0^{t_2} dt'' \langle z(t')z(t'')\rangle$$
$$= \int_0^{t_1} dt' \int_0^{t_2} dt'' e^{-ik_*(t'-t'')} \langle z(\mathbf{e_1})z(\mathbf{e_2})\rangle$$

$$\langle z(\mathbf{e_1})z(\mathbf{e_2})\rangle = \sum_l \frac{2l+1}{4\pi} C_l P_l(\mathbf{e}_1 \cdot \mathbf{e}_2)$$

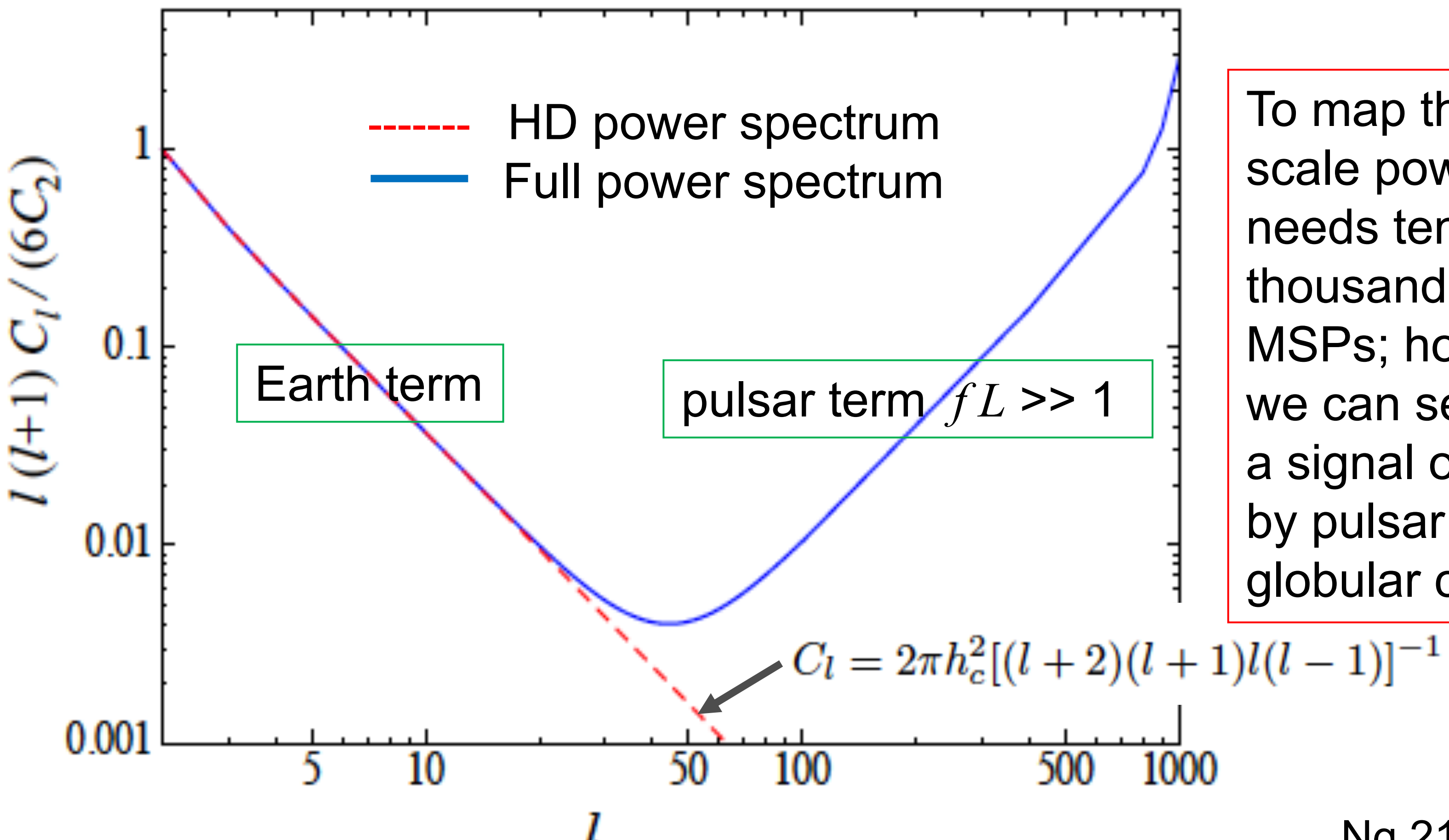

To map this small-scale power needs tens of thousands of MSPs; however, we can search for a signal of close-by pulsar pairs in globular clusters

Ng 21

Conclusion

- GWB is a main goal in GW experiments
- GWB monopole and Doppler dipole
- GWB anisotropy and polarization
- Correlate with other cosmological data such as LSS, CMB
- GWB is a deep probe into the very early Universe
- Pulsar-timing-arrays saw the GW monopole? If so, then the game may have started…
- Beyond Einstein gravity, see Bernardo's talk

The Future is “Dark”

The Future is Illuminating